STABILITY OF A TETHERED SATELLITE FORMATION ABOUT THE LIKINS-PRINGLE EQUILIBRIA

THESIS

Ayhan Tuncay, 1 LT, TUAF
AFIT/GSO/ENY/02-4

DEPARTMENT OF THE AIR FORCE
AIR UNIVERSITY

AIR FORCE INSTITUTE OF TECHNOLOGY

Wright-Patterson Air Force Base, Ohio

The views expressed in this thesis are those of the author and do not reflect the official policy or position of the Department of Defense, the U. S. Government, or the Government of Turkish Republic.

AFIT/GSO/ENY/02-4

STABILITY OF A TETHERED SATELLITE FORMATION ABOUT THE LIKINS-PRINGLE EQUILIBRIA

THESIS

Presented to the Faculty

Department of Aeronautics and Astronautics

Graduate School of Engineering and Management

Air Force Institute of Technology

Air University

Air Education and Training Command

In Partial Fulfillment of the Requirements for the

Degree of Master of Science (Space Operations)

Ayhan Tuncay, BS

1 LT, TUAF

March 2002

AFIT/GSO/ENY/02-4

STABILITY OF A TETHERED SATELLITE FORMATION ABOUT THE LIKINS-PRINGLE EQUILIBRIA

Ayhan Tuncay, BS
1 LT, TUAF

Approved:

Steven G Tragesser	15 MAR 02
Steve G. Tragesser (Chairman)	date
William E. Wiesel	15 Mar 02
William E. Wiesel (Member)	date
Richard G. Cobb	15 MAR 02
Richard G. Cobb (Member)	date

Acknowledgements

In many cases this research was clearly an immense task and it says much for the hard and skillful work of the contributors that the whole process was completed in a year. I wish to acknowledge my many friends and instructors at AFIT, and elsewhere who gave help and encouragement in completing this research. To these individuals I express my most sincere appreciation.

There were many hard-working people behind the scenes. I especially appreciate the enthusiastic support that I have received from my research advisor Steven G. Tragesser. I also would like to thank him for his creative ideas, great patience and a great deal of excellent advice. I am so grateful to Lt Hakan San not only for many helpful discussions, but also his constructive criticism and suggestions. I have to admit that this research would not be completed without Hakan's contributions and his constructive criticism and suggestions. I would also like to thank my committee members, Dr. William E. Wiesel and Maj. Richard G. Cobb.

Finally, it is always a joy and a privilege to express my gratitude to my beloved wife and our child for their love, support and emotional sustenance during the completion of this research.

Ayhan TUNCAY

Table of Contents

Page

List of Figures

Figure Page

Abstract

Previous efforts have been directed at the guidance and control of free flying satellites clusters using reaction thrusters. A Tethered Formation of Satellites with distributed sensors has great potential to enhance surveillance and imaging of earth objects. To maintain the shape of the formation and keep the tethers in tension, the system needs to be spinning. To take the advantages of distributed sensors, the spin axis of the formation must have a component on nadir direction. General study has been focused on a planar formation and the results showed that Earth pointing configurations are not stable. This study demonstrates that spin stabilization and the use of gravity gradient for formation flight with tethered satellites reduce the necessity of thrusters for station keeping maneuvers. A tethered satellite formation, which consists of three satellites at the corners of an equilateral triangle, and two end bodies at the opposite side of this triangular plane is studied to obtain the stability based on the Likins-Pringle equilibrium for rigid satellites, for long period. Parameters that affect the stability of the tethered formation and the application of the Likins-Pringle relative equilibrium to the tethered formation are presented in this study. Equilibrium conditions for the tethered formation and the stable formation design for a long period are demonstrated. Depending on the size of the formation and the mass ratio of the satellites to end bodies, long-term stability is achievable for a continuously earth-pointing tethered satellite formation.

STABILITY OF A TETHERED SATELLITE FORMATION

ABOUT THE LIKINS-PRINGLE EQUILIBRIA

I. Introduction

1.1 Motivation

Using a satellite cluster for a space mission has become an interesting subject in recent years. Using several small satellites in a cluster instead of a large satellite has numerous advantages. For some space missions such as surveillance or terrain mapping, in order to improve resolution, the sensors must have a large aperture, which directly increases the size and the mass of the satellite. On the other hand the size of the satellite is limited by the capability of the launch vehicles. However with distributed sensors, it may be possible to achieve a resolution that cannot be attained with a single satellite.

In some applications, each small satellite in the cluster communicates with the others and shares the processing, information and mission functions. A cluster of this kind might be used to form a large aperture. While current developments may allow apertures the size of meters, it may be possible to form an aperture with the size of kilometers with distributed satellites. This feature can be useful for space based radar and remote sensing missions, which require large aperture products to achieve acceptable area coverage and precision or lower resolution [1].

Satellites formations have received a lot of attention in recent years and have been the subject of many research efforts. The U.S. Air Force is exploring formations for use in surveillance, passive radiometry, terrain mapping, navigation, communications and ground target identification as mentioned in the research of Irvin [2].

Unfortunately to keep the group of satellites in relatively close proximity in a formation may require significant fuel expenditure [3]. Station keeping maneuvers and burns to keep the formation are due to the perturbations and unmodeled forces. An alternate concept is to form a formation with small satellites, using tethers between these satellites in the formation [4]. Instead of using thrusters for each satellite for all station keeping maneuvers, using a tether between satellites would reduce the fuel consumption.

1.2 Problem Statement

Although using tethers between satellites in the formation is beneficial to reduce the fuel consumption, a stable configuration must be found in order to make the idea practical. All the satellites in the formation have different forces than a single satellite in orbit. While the main force is the gravitational force on the satellites, there are also tension forces through the tether on the satellites in the formation. To keep the formation in a desired configuration, tethers between the satellites must be in tension. These tension forces will help to rigidize the tethered satellite system and keep the formation from collapsing or otherwise altering its shape.

The center of mass of the formation follows an orbital path that is assumed to be elliptical. However satellites in the tethered formation have affects on each other with the

tension force through the tethers between them. Thus the dynamics of a tethered satellite formation are affected by the tensional forces. These additional forces on a satellite cause the satellite to behave in a non-Keplerian manner [5] [6].

Since the studied application of the tethered formation is Earth surveillance and sensing, the system must be designed so the sub satellites are widely distributed about the nadir directions. Previous studies have been focused on a planar formation and the results showed that Earth pointing configuration is not stable.

For the stability of the tethered formation, to use the benefits of the gravity gradient forces, two end bodies are placed at the opposite side of the triangular plane of the satellites as in Figure 1.1.

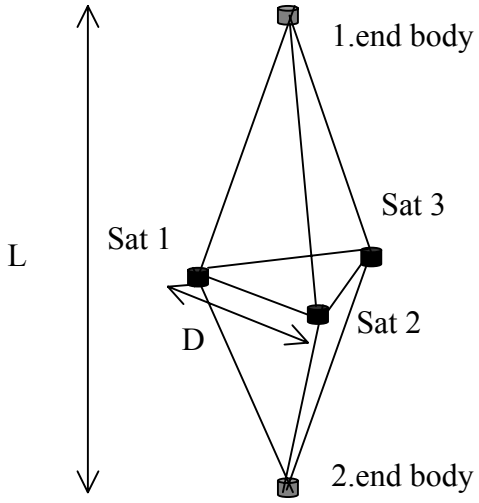

Fig 1.1 Tethered Formation

1.3 Objectives

The goal of this thesis is to demonstrate a stable tethered satellite formation for a long period. This thesis focused on a closed-loop formation with two end bodies at the opposite sides of the triangular plane of the satellites as shown in Fig1.1. Since the application of the tethered formation is Earth surveillance and sensing, the system will be designed so the sub satellites will be widely distributed about the nadir directions. To find the stability condition and the equilibrium position of the tethered formation about the nadir direction, analysis of Likins-Pringle relative equilibrium and the possibility of using this equilibrium will be addressed.

Stability of the formation will be analyzed for a range of spin rates, formation sizes and formation masses. Due to the complexity of the dynamics, the equations of motion will be solved numerically. Parameters that affect the stability of the formation will be presented with the results.

II. Background and Previous Research

In this chapter benefits of using tethers in space will be presented with some possible applications. Research about tethered satellite systems and the dynamics and modeling of tethers will be presented.

2.1 Possible Space Missions With Tethers

Over the last two decades, engineers have realized the potential benefits of tethers in space. It has been pointed out that it is possible to use a tether between different bodies for many space missions.

Using tethers between distributed satellites to form a large aperture is a possible way of increasing the capability of a surveillance system. The physical size of an aperture, which directly relates to the achievable resolution, is limited by the launch vehicle capacity. On the other hand, the properties of an earth surveillance system can be increased with distributed small satellite connected with tethers.

Creating artificial gravity with the rotation of two bodies connected with tethers is an important issue for long duration manned space flights. To separate an orbital station into two parts connected by a tether and spin the system about its center of mass is the basic idea of creating artificial gravity. As it is mentioned in reference Dynamics of Space Tether Systems, Chobotov was the first investigator to present a detailed dynamic

analysis of this motion and Gemini 11 was the first spacecraft to demonstrate this concept in 1966, which connected to the rocket stage Agena with tether [7].

Docking of the orbiter to a remote tethered unit, which is separated with a long tether from the station, is one possible way to avoid docking impacts on the station and to save considerable amount of fuel during maneuvering in this step [7].

An orbiting interferometer, which has different receivers connected by tethers could be beneficial to provide high resolution.

Scientific measurements in the atmosphere at altitudes of about 100 km could be possible with tethered units, which are connected to the orbiter at higher altitude. This altitude of atmosphere is not accessible for aircraft because of the low density and also is not accessible for the spacecraft because of the high density for space missions at the same time. However an atmospheric probe, which is connected to the orbiter with a very long tether can solve this problem [7].

A tethered unit, which can be deployed from a spacecraft into a dense atmospheric layer can transfer the aerodynamic breaking force to the vehicle through the tether. After the desired reentry conditions are reached, the tethered unit can be separated from the orbiter. During this maneuver it is possible to save a considerable amount of fuel [7] [8].

Another useful application of tethers in space is the electrodynamic tether system, which has a conducting tether deployed from the station. Interaction between the tether and the geomagnetic field of earth could supply enough power for orbital maneuvering of the station [7].

2.2 Previous Research

There has been a great deal of research about tethers in space over the past two decades. Most of this research is related to the dynamics and modeling of the tethers and tethered satellite systems. This research will be presented in two different sections.

2.2.1 Tether Modeling

In order to design missions and predict the behaviour of the tethered satellite system, engineers had to develop some techniques to model the tether. While most of the researchers have considered massless tether for the satellite formation, some engineers have modeled the tether with different techniques. To model the tethers, which are used in tethered satellite system, some methods must be used to discritize the continuous tether. There are some basic differences between discrete and continuous systems. Primarily, discrete systems have a finite number of degrees of freedom, and continuous systems have an infinite number of degrees of freedom. Discrete systems are governed by ordinary differential equations while continuous systems by partial differential equations [9]. The difficulties in obtaining closed-form solutions to problems of continuous systems can be summarized as the difficulty of solving the partial differential equations of the continuous systems. So to get closed-form solutions for a tether, it should be discritized by some techniques. Approximate solutions for the continuous systems generally involve discritization of the systems, and these approximate solutions differ from each other with the discritization technique that is used [10].

The most commonly used techniques to discretize the continuous tether are the assumed mode method and discritization with particles (bead model). Discritization with

particles method models the tether with small masses connected with massless tethers. All the external forces can be applied to these small particles and it is possible to obtain ordinary differential equations.

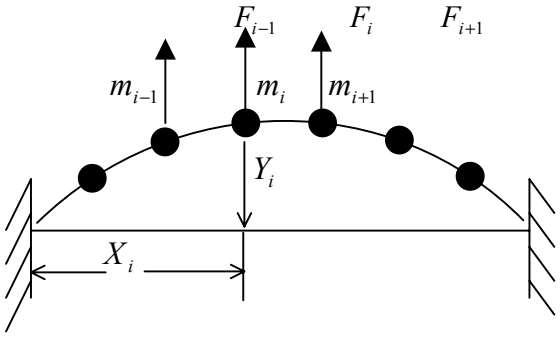

Figure 2.1 Bead Model for Tether [7]

Forces on the particles can be shown as:

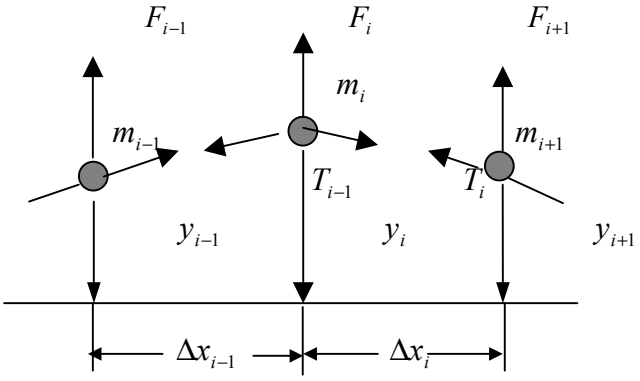

Figure 2.2 Forces on the Tether [7]

The assumed modes method discretizes the continuous system prior to the derivations of the equations of motion. The solution for the system is assumed in a finite series form of space-dependent functions, but the coefficients are time-dependent

generalized coordinates instead of being constant. This series is substituted in a kinetic and potential energy, thus reducing them to discrete form, and the equations of motion are derived by means of Lagrange's equations [10].

Biesbroek et. al.[11] has compared the results of two different modeling methods of tethers. These two methods are the bead model and the continuum tether model. A comparison of two computer simulation models has been given by the author. These two simulations are TETSIM (bead model) and DATES (continuum tether). In this report it is pointed out that when a tether is modeled with beads, which are connected by inextensible and massless lines, it is possible to obtain accurate results for many applications. And also it is possible to reduce the simulation time with bead model, even if many beads are used.

Modi et. al.[12] have studied the dynamics and control of tethered spacecraft during deployment and retrieval. In this research, the author has examined some of the important aspects of the other studies about tethered systems, which include the modeling of tethers and system dynamics and control.

Dynamic behavior of a tethered system in elliptical orbits has been investigated by Takeichi et. al.[13]. For this study, the tethered system is modeled with a combination of rigid bodies, and the effects of tether elasticity and atmospheric drag is studied.

Dynamical characteristics of a tethered stabilized satellite have been researched by Ashenberg et.al.[14]. It is pointed out by the author that, attaching a tether with a mass at the opposite of the satellites would increase the stability of the satellite. In this work, stability characteristics of a tethered satellite have been presented.

Zhu et. al.[14] has focused on the dynamical model and the mathematical formulations of tethered systems with two satellites on a line. He presented two dynamical models and formulations in his report for the tethered satellite system, which has a subsatellite and one main satellite with a point mass much greater than the subsatellite. For the first model, an elastic continuum is used to model the tether with mass and he has assumed the tether would remain straight. In the second model tether between the main satellites and subsatellites is modeled with discrete masses, which are connected with massless springs. For the second model the main satellite has much greater mass than the subsatellite, so he assumed that the center of mass of the tethered system is located at the main satellite.

2.2.2 Multi- Satellites

Although most research has focused on the tethered satellite systems with two end bodies, there are some others which have focused on the tethered systems with multibodies such as Kalantzis et. al. [15]. In this report the equations of motion for a multi-satellite tethered system in a Keplerian orbit are derived. His model considers a multi-satellite system which the satellites in the formation are connected to each other by flexible tethers. Equations for the model have been derived using the Lagrangian approach, and a continuum model has been used for tethers. Assumed mode methods is used to discritize the deformations of the tethers.

DeCou[16] has focused on an orbiting stellar interferometer which has three distributed satellites at the corners of an equilateral triangle. This satellite formation system is determined that it is spinning around the axis, which is perpendicular to the

formation plane. Centrifugal force created by the spinning of the formation keeps the tether taut. For this system, gravity gradient, solar radiation pressure and thermal expansion forces are taken into account as a perturbation forces. Tethers between the satellites are determined under the influence of the centrifugal force and modeled with small point masses. Solution for the static problem has been obtained by deriving the nonlinear differential equations, which relate the position of each tether point to the tension at each point. Numerical solutions for these equations are presented. For this study it is assumed that three satellites at the corners of the equilateral triangle follow a circular path by spinning the formation around the axis perpendicular to the plane. The spin rate for DeCou's formation is much greater than the orbital mean motion, so the spin axis maintains a nearly inertially fixed direction.

Tragesser [4] has focused on a satellite ring as DeCou. Tethers are used to reduce propulsive station keeping maneuvers to maintain the formation. Earth surveillance is the desired application for this project, so the tethered satellite system is designed so the relative spin axis of the formation has a component along nadir direction. Unlike DeCou's work, Tragesser's formation spins at a rate comparable to the orbital motion. Conical equilibrium has been chosen to get the maximum projected area onto the earth for surveillance besides stability. Satellite formation has composed of three satellites at the corners of an equilateral triangle and the tethers between these satellites have been modeled with an arbitrary number of point masses. A common law of elasticity has been used to find the tension force on the tether. Likins-Pringle relative equilibria [17] for the conical case has been used to find the angle between the spin axis and orbit normal to

maximize the projected area onto the earth. As a result of this paper it is observed that the rigid body equilibrium doesn't give the same stability results for flexible systems.

Williams and Moore have examined the feasibility of a multi-tether system that is very similar to the one presented here. They focused on tethered satellite formations which have the spin axis aligned with the nadir direction. To use the gravity gradient effect for stability, they have studied a configuration with four satellites on the plane perpendicular to the spin axis and two anchor satellites at the opposite sides of this plane. This tethered satellite configuration also has a central tether between these two anchor satellites. In this research all the tethers are assumed as massless and remain straight during the motion. Clohessy-Wiltshire equations are used to describe the equations of motion of the satellites with respect to the center of mass of the entire system. The authors presented a stable configuration with small periodic oscillations of two degrees about the velocity vector of the reference orbit [20].

This thesis builds on this previous work to show that the nadir-oriented formation of Williams and Moore is actually an approximation of the Likins-Pringle relative equilibria for rigid bodies. Using this theory, this thesis demonstrates that there exists a range of stable configurations within a couple degrees of nadir.

III. Methodology

In this chapter, modeling of the tethered satellite system will be presented. Orientation of the TSS will be given and for the stability of the formation system, spin stabilization on orbit will be explained. Likins-Pringle relative equilibrium concept for the spinning rigid body will be revisited and it will be adapted to the tethered satellite system.

3.1 Nominal Design

The formation design for this thesis is comprised of three satellites at the corners of an equilateral triangle and two end masses at the opposite side of this triangular plane with the same distance from the triangular plane. The three satellites and the two end bodies are considered as point masses. Tethers are placed between the satellites and between the end bodies and satellites with the same properties as shown in Figure 3.1 in the body fixed reference frame.

Because the formation is axisymmetrical, the center of mass of the system is at the center of the triangular plane. In the Figure 3.1, L represents the distance between two end bodies and D is used for the distance between the satellites. All the tethers in the formation are assumed as extensible and remain straight during the motion. Modeling of the tethers will be discussed in Chapter 4 with more detail.

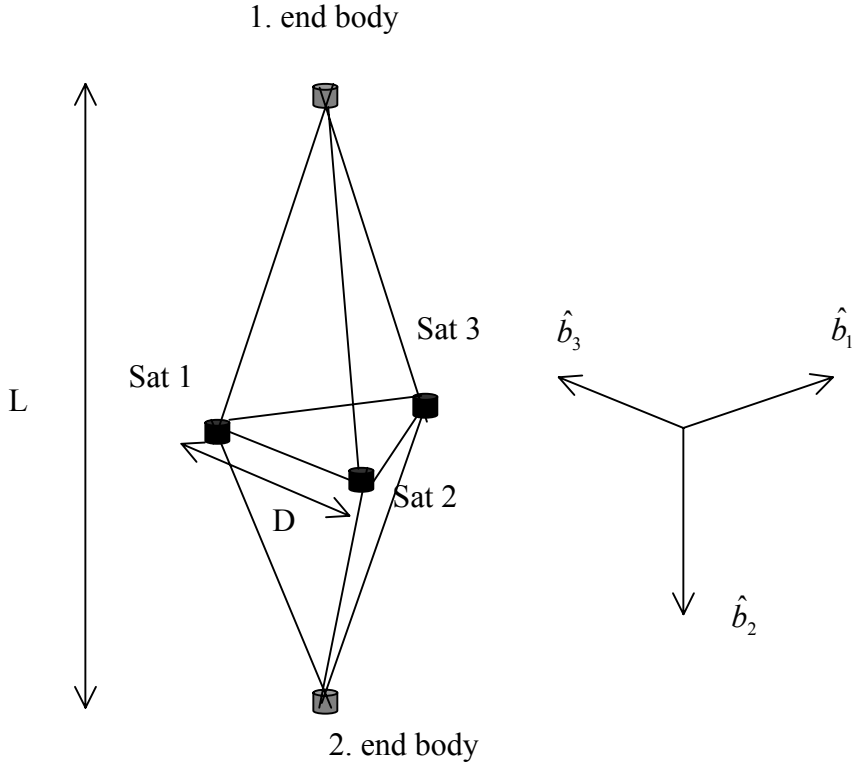

Figure 3.1 TSS Model

The three satellites are at the corners of an equilateral triangle can be shown in Figure 3.2.

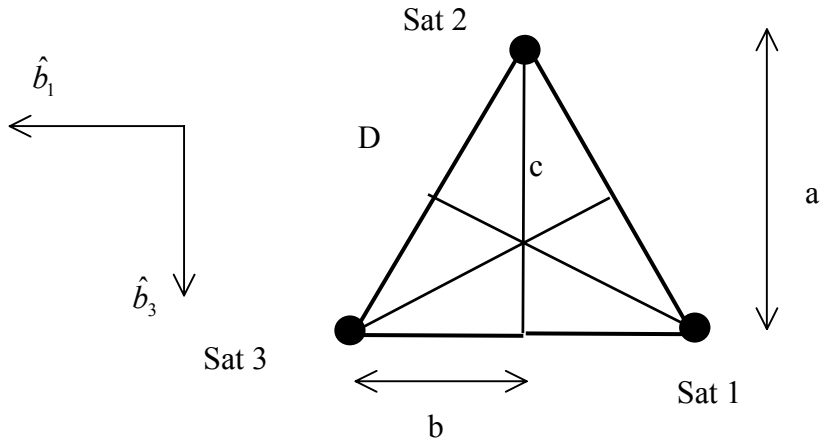

Figure 3.2 Satellites on triangular plane

where c is the distance between the satellites and the center of mass and b is equals to ½ of the distance between satellites.

Positions of the satellites and the end bodies with respect to the center of mass in the body frame F_b can be written by geometry of the system as:

$$
\begin{aligned}
&(\text{a}) \quad \bar{r}_{e1}^{b} = \begin{bmatrix} 0 & -L/2 & 0 \end{bmatrix} \\
&(\text{b}) \quad \bar{r}_{e2}^{b} = \begin{bmatrix} 0 & L/2 & 0 \end{bmatrix} \\
&(\text{c}) \quad \bar{r}_{s1}^{b} = \begin{bmatrix} -D/2 & 0 & D/(2\sqrt{3}) \end{bmatrix} \\
&(\text{d}) \quad \bar{r}_{s2}^{b} = \begin{bmatrix} 0 & 0 & -D/\sqrt{3} \end{bmatrix} \\
&(\text{e}) \quad \bar{r}_{s3}^{b} = \begin{bmatrix} D/2 & 0 & D/(2\sqrt{3}) \end{bmatrix}
\end{aligned} \tag{3.1}
$$

where $\bar{r}_{e1}^{b}$ and $\bar{r}_{e2}^{b}$ denotes the two end bodies, and $\bar{r}_{s1}^{b}$, $\bar{r}_{s2}^{b}$ and $\bar{r}_{s3}^{b}$ denotes three satellites. By using these equations, the distance of each mass to the center of mass can be found as:

$$\left|\bar{r}_{e1}^{b}\right| = \left|\bar{r}_{e2}^{b}\right| = L/2 \tag{3.2}$$

$$\left|\bar{r}_{s1}^{b}\right| = \left|\bar{r}_{s2}^{b}\right| = \left|\bar{r}_{s3}^{b}\right| = D/\sqrt{3} \tag{3.3}$$

For the orientation of the formation in body frame the inertias of each mass with respect to the center of mass are:

$$I_{e1} = m_{eb}\begin{bmatrix} L^2/4 & 0 & 0 \\ 0 & 0 & 0 \\ 0 & 0 & L^2/4 \end{bmatrix} \tag{3.4}$$

$$I_{e2} = m_{eb}\begin{bmatrix} L^2/4 & 0 & 0 \\ 0 & 0 & 0 \\ 0 & 0 & L^2/4 \end{bmatrix} \tag{3.5}$$

$$I_{s1} = m_{s1}\begin{bmatrix} \frac{D^2}{12} & 0 & -\frac{D^2}{4\sqrt{3}} \\ 0 & \frac{D^2}{3} & 0 \\ -\frac{D^2}{4\sqrt{3}} & 0 & \frac{D^2}{4} \end{bmatrix} \tag{3.6}$$

$$I_{s2} = m_{s2}\begin{bmatrix} D^2/3 & 0 & 0 \\ 0 & D^2/3 & 0 \\ 0 & 0 & 0 \end{bmatrix} \tag{3.7}$$

$$I_{s3} = m_{s3}\begin{bmatrix} \frac{D^2}{12} & 0 & \frac{D^2}{4\sqrt{3}} \\ 0 & \frac{D^2}{3} & 0 \\ \frac{D^2}{4\sqrt{3}} & 0 & \frac{D^2}{4} \end{bmatrix} \tag{3.8}$$

where m_{e1} and m_{e2} denotes the mass of the end bodies and m_{si} denotes the mass of the satellites. For the TSS model mass of the satellites are equal to each other, and so the mass of the satellites can be denoted as m_s and the mass of the end bodies can be denoted as m_e. Therefore the total inertia of the system is:

$$I = \begin{bmatrix} \frac{m_e L^2}{2} + \frac{D^2 m_s}{2} & 0 & 0 \\ 0 & D^2 m_s & 0 \\ 0 & 0 & \frac{m_e L^2}{2} + \frac{D^2 m_s}{2} \end{bmatrix} = \begin{bmatrix} I_t & 0 & 0 \\ 0 & I_a & 0 \\ 0 & 0 & I_t \end{bmatrix} \tag{3.9}$$

The tethered satellite system, which consists of distributed satellite on a equilateral triangle, must rotate about the axis perpendicular to the plane to keep the tether in tension and to rigidize the system. Without spinning it is not possible to maintain

the stability of the satellite formation with flexible tethers. It is possible to rigidize the system by spinning the formation about the axis perpendicular to the plane of the satellites.

There are three types of equilibria for the spinning rigid body, these are cylindrical, hyperbolic and conical equilibria (Fig 3.3). For the cylindrical and hyperbolic cases, because of the direction of the spin axis, the satellites' path forms a line when projected onto the Earth's surface. These formations do not take advantage of the distribution of sensors. On the other hand for the conical case, the spin axis has a component in the nadir direction, so the projection of the formation enhances Earth sensing capability.

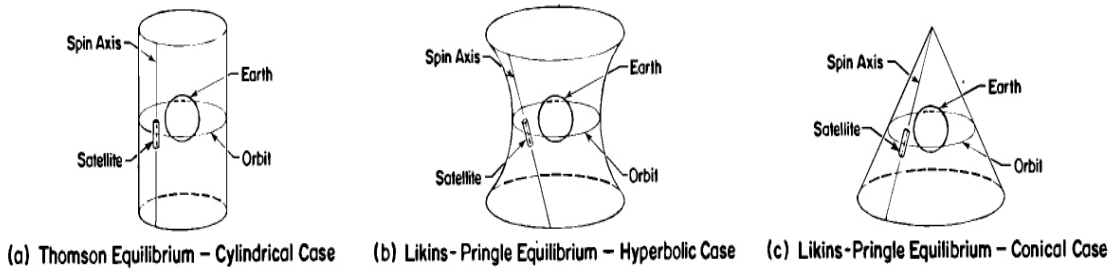

Figure 3.3 Types of relative equilibrium for a spinning symmetrical satellite [17]

This thesis will focus on the conical type of equilibria to increase the projection of the satellite on the Earth's surface. In the following sections Likins-Pringle relative equilibrium concept will be represented and then adapted to the satellite formation with flexible tethers.

For an axisymmetrical satellite with axial and transverse inertias I_a and I_t respectively, the simplest case is to maintain the spin axis nominally normal to the orbit, without any gravity gradient torque on the satellite [17].

3.1.1 Thomson Equilibrium

An explanation of the Thomson Equilibrium will help to explain the Likins-Pringle conical equilibrium, used in the formation design. For this equilibrium, the satellite is assumed an axisymmetrical rigid body with the transverse and axial inertias I_t and I_a respectively. The reference motion for the Thomson equilibrium is in Figure 3.4

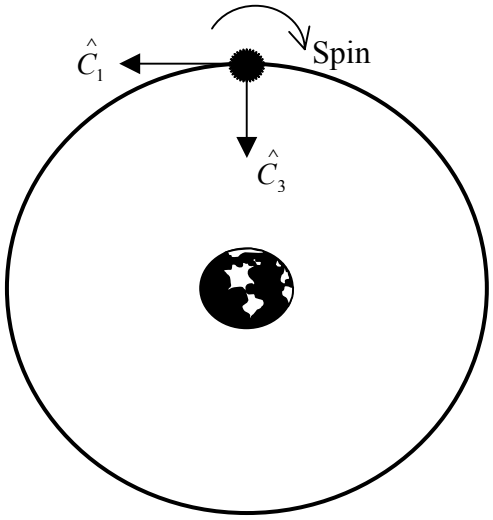

Figure 3.4 Thomson equilibrium [17]

For this reference motion four frames are used, which are the body frame, orbital frame, inertial frame, and reference spin frame.

F_b : Body fixed principal-axis frame

F_c : Orbital frame

F_i : Inertial frame

F_a : Reference spin frame

The reference spin frame, F_a, rotates about the $\hat{a}_2$ axis with respect to F_i at rate ν. Transformation between the reference spin frame and inertial frame is:

$$R^{ai} = R_2(\nu t) = \begin{bmatrix} \cos(\nu t) & 0 & -\sin(\nu t) \\ 0 & 1 & 0 \\ \sin(\nu t) & 0 & \cos(\nu t) \end{bmatrix} \tag{3.10}$$

where R^{ai} indicates the transformation between the reference spin frame F_a and F_i , and R_i indicates the rotation matrix about i th axis.

For the reference motion, body frame F_b and the reference spin frame F_a are aligned, but with small excursions α. The linearized transformation between these frames is:

$$R^{ba} = \begin{bmatrix} 1 & \alpha_3 & -\alpha_2 \\ -\alpha_3 & 1 & \alpha_1 \\ \alpha_2 & -\alpha_1 & 1 \end{bmatrix} \tag{3.11}$$

The relationship between the orbital frame F_c and the inertial frame F_i is:

$$R^{ci} = R_2(-\omega_c t) = \begin{bmatrix} \cos(\omega_c t) & 0 & \sin(\omega_c t) \\ 0 & 1 & 0 \\ -\sin(\omega_c t) & 0 & \cos(\omega_c t) \end{bmatrix} \tag{3.12}$$

where ω_c is the nominal motion.

By using these relationships, transformation between the body frame F_b and the orbital frame F_c can be calculated:

$$R^{bc} = R^{ba} R^{ai} R^{ic} = R^{ba} R^{ai} (R^{ci})^T \tag{3.13}$$

From equation (3.10) and (3.12)

$$R^{ai} (R^{ci})^T = R_2(\nu t) R_2(\omega_c t) = R_2[(\nu + \omega_c)t] \tag{3.14}$$

Substitution (3.14) into (3.13) yields:

$$R^{bc} = \begin{bmatrix} 1 & \alpha_3 & -\alpha_2 \\ -\alpha_3 & 1 & \alpha_1 \\ \alpha_2 & -\alpha_1 & 1 \end{bmatrix} \begin{bmatrix} \cos((\nu + \omega_c)t) & 0 & -\sin((\nu + \omega_c)t) \\ 0 & 1 & 0 \\ \sin((\nu + \omega_c)t) & 0 & \cos((\nu + \omega_c)t) \end{bmatrix} \tag{3.15}$$

The reference satellite is an axisymmetrical rigid body. The axial inertia is I_a and transverse inertia is I_t, and because of the symmetry $I_1 = I_3 = I_t$ and $I_2 = I_a$. The angular velocity of this satellite with respect to the inertial frame can be written using the relations between the frames. The body frame is aligned with the reference spin frame with small excursions and the reference frame rotates about the $\hat{a}_2$ axis with respect to the inertial frame.

$$\overline{\omega}^{bi} = \overline{\omega}^{ba} + \overline{\omega}^{ai} \tag{3.16}$$

For small α_i this can be approximated by:

$$\overline{\omega}^{bi} = \dot{\alpha}_1 \hat{b}_1 + \dot{\alpha}_2 \hat{b}_2 + \dot{\alpha}_3 \hat{b}_3 + \nu \hat{a}_2 \tag{3.17}$$

The last term of this equation can be transformed into the body frame by using the transformation between body frame and reference spin frame as:

$$\nu\hat{a}_2 = R^{ba}\begin{bmatrix}0\\ \nu\\ 0\end{bmatrix} = \begin{bmatrix}1 & \alpha_3 & -\alpha_2\\ -\alpha_3 & 1 & \alpha_1\\ \alpha_2 & -\alpha 1 & 1\end{bmatrix}\begin{bmatrix}0\\ \nu\\ 0\end{bmatrix} \tag{3.18}$$

$$\nu\hat{a}_2 = \alpha_3\nu\hat{b}_1 + \nu\hat{b}_2 - \alpha_1\nu\hat{b}_3 \tag{3.19}$$

By substituting the equation (3.19) into equation (3.17), the angular velocity of the satellite in body frame is:

$$\overline{\omega}^{bi} = \omega_1^{bi}\,\hat{b}_1 + \omega_2^{bi}\,\hat{b}_2 + \omega_3^{bi}\,\hat{b}_3 \tag{3.20}$$

$$\overline{\omega}^{bi} = \dot{\alpha}_1\hat{b}_1 + \dot{\alpha}_2\hat{b}_2 + \dot{\alpha}_3\hat{b}_3 + \alpha_3\nu\hat{b}_1 + \nu\hat{b}_2 - \alpha_1\nu\hat{b}_3 \tag{3.21}$$

where ω_i^{bi} indicates the components of the angular velocity for $\hat{b}_i$ axis. Equating components of (3.20) and (3.21) gives:

$$\text{(i)}\quad \omega_1^{bi} = \dot{\alpha}_1 + \alpha_3\nu$$

$$\text{(ii)}\quad \omega_2^{bi} = \dot{\alpha}_2 + \nu$$

$$\text{(iii)}\quad \omega_3^{bi} = \dot{\alpha}_3 - \alpha_1\nu \tag{3.22}$$

To find the equations of motion it is needed to calculate the gravity gradient torque for the reference satellites. Gravity gradient torque depends on the position of the satellite with respect to the inertial frame and the inertias of the satellite. Gravity gradient torque of the satellite in the body frame is:

$$\overline{M} = M_1\,\hat{b}_1 + M_2\,\hat{b}_2 + M_3\,\hat{b}_3 \tag{3.23}$$

where M_i is a scalar value and indicates the magnitude of the gravity gradient torque for the $\hat{b}_i$ axis. The components of the gravity gradient torque are given by [18]:

$$(\text{i}) \quad \mathrm{M}_1 = \frac{3\mu}{r^5}\mathrm{YZ}(I_t - I_a)$$

$$(\text{ii}) \quad \mathrm{M}_2 = \frac{3\mu}{r^5}\mathrm{XZ}(I_t - I_t)$$

$$(\text{iii}) \quad \mathrm{M}_3 = \frac{3\mu}{r^5}\mathrm{XY}(I_a - I_t) \tag{3.24}$$

where X, Y and Z are the position of the satellite in body frame with respect to the inertial frame:

$$\bar{r}^b = \mathrm{X}\hat{b}_1 + \mathrm{Y}\hat{b}_2 + \mathrm{Z}\hat{b}_3 \tag{3.25}$$

These coordinates can be found with the transformation between the orbital frame and the body frame as:

$$\bar{r} = r\hat{c}_3 = R^{bc}\begin{bmatrix}0\\0\\r\end{bmatrix} \tag{3.26}$$

$$\bar{r}^b = \begin{bmatrix}1 & \alpha_3 & -\alpha_2\\ -\alpha_3 & 1 & \alpha_1\\ \alpha_2 & -\alpha_1 & 1\end{bmatrix}\begin{bmatrix}\cos((\nu+\omega_c)t) & 0 & -\sin((\nu+\omega_c)t)\\ 0 & 1 & 0\\ \sin((\nu+\omega_c)t) & 0 & \cos((\nu+\omega_c)t)\end{bmatrix}\begin{bmatrix}0\\0\\r\end{bmatrix} \tag{3.27}$$

$$\bar{r}^b = \begin{bmatrix}-r\sin(\nu+\omega_c)t - \alpha_2\cos(\nu+\omega_c)t\\ \alpha_3 r\sin(\nu+\omega_c)t + \alpha_1 r\cos(\nu+\omega_c)t\\ -\alpha_2 r\sin(\nu+\omega_c)t + r\cos(\nu+\omega_c)t\end{bmatrix}\begin{bmatrix}\hat{b}_1\\ \hat{b}_2\\ \hat{b}_3\end{bmatrix} \tag{3.28}$$

Therefore the coordinates X, Y and Z are:

$$(\text{i}) \quad \mathrm{X} = -r\sin(\nu+\omega_c)t - \alpha_2\cos(\nu+\omega_c)t$$

$$(\text{ii}) \quad \mathrm{Y} = \alpha_3\, r\sin(\nu+\omega_c)t + \alpha_1 r\cos(\nu+\omega_c)t$$

$$(\text{iii}) \quad \mathrm{Z} = -\alpha_2 r\sin(\nu+\omega_c)t + r\cos(\nu+\omega_c)t \tag{3.29}$$

Substituting these values into the gravity gradient equations and ignoring the higher order terms yields:

$$\mathrm{M}_1 = \frac{3\mu}{r^5} r^2 (I_t - I_a)\left\{\alpha_3 \sin[(\nu+\omega_c)t]\cos[(\nu+\omega_c)t] + \alpha_1 \cos^2[(\nu+\omega_c)t]\right\} \quad (3.30)$$

$$\mathrm{M}_2 = 0 \quad (3.31)$$

$$\mathrm{M}_3 = \frac{3\mu}{r^5} r^2 (I_a - I_t)\left\{-\alpha_3 \sin^2[(\nu+\omega_c)t] - \alpha_1 \sin[(\nu+\omega_c)t]\cos[(\nu+\omega_c)t]\right\} \quad (3.32)$$

For a circular reference orbit the first term can be simplified as:

$$\frac{\mu}{r^5} r^2 = \frac{\mu}{r^3} = \omega_c \quad (3.33)$$

The equations of motion can be written [18]:

$$\begin{aligned}
&(\text{i}) \quad I_t \dot{\omega}_1^{\,bi} + (I_t - I_a)\omega_2^{bi}\omega_3^{bi} = \mathrm{M}_1 \\
&(\text{ii}) \quad I_a \dot{\omega}_2^{\,bi} + (I_t - I_t)\omega_1^{bi}\omega_3^{bi} = \mathrm{M}_2 \\
&(\text{iii}) \quad I_t \dot{\omega}_3^{bi} + (I_a - I_t)\omega_1^{bi}\omega_2^{bi} = \mathrm{M}_3
\end{aligned} \quad (3.34)$$

where the term $\dot{\omega}_i^{bi}$ indicates the derivation of the angular velocity and can be written by taking the derivatives of the equations (3.22).

$$\begin{aligned}
&(\text{i}) \quad \dot{\omega}_1^{\,pi} = \ddot{\alpha}_1 + \dot{\alpha}_3 \nu \\
&(\text{ii}) \quad \dot{\omega}_2^{\,pi} = \ddot{\alpha}_2 \\
&(\text{iii}) \quad \dot{\omega}_3^{\,pi} = \ddot{\alpha}_{31} - \dot{\alpha}_1 \nu
\end{aligned} \quad (3.35)$$

Substituting the gravity gradient torques and the derivatives of the angular velocity into equations (3.34), (Appendix B) the linearized equations of motion can be written as:

$$\ddot{\alpha}_1 + (1-k_t)\nu\dot{\alpha}_3 + k_t\nu^2\alpha_1 + 3\omega_c^2 k_t(\alpha_1 c + \alpha_3 s)c = 0 \tag{3.36}$$

$$\ddot{\alpha}_2 = 0 \tag{3.37}$$

$$\ddot{\alpha}_3 - (1-k_t)\nu\dot{\alpha}_1 + k_t\nu^2\alpha_3 + 3\omega_c^2 k_t(\alpha_1 c + \alpha_3 s)s = 0 \tag{3.38}$$

where:

$$s = \sin(\nu + \omega_c)t \qquad c = \cos(\nu + \omega_c)t \qquad \omega_c = \sqrt{\frac{\mu}{R^3}} \quad \text{and}$$

$$k_t = \frac{I_a - I_t}{I_t} \tag{3.39}$$

The linearized equations of motion include time variable coefficients because of the nominal motion of the satellite and the reference spin rate. It is possible to simplify these equations by transforming them to a new set of coordinates that will eliminate the periodic coefficients. The new parameters are defined by Hughes as[17]:

$$\text{(i)} \quad \gamma_1(t) \triangleq \alpha_1(t)\cos(\nu + \omega_c)t + \alpha_3(t)\sin(\nu + \omega_c)t$$

$$\text{(ii)} \quad \gamma_2(t) \triangleq \alpha_2(t)$$

$$\text{(iii)} \quad \gamma_3(t) \triangleq -\alpha_1(t)\sin(\nu + \omega_c)t + \alpha_3(t)\cos(\nu + \omega_c)t \tag{3.40}$$

Substituting these new parameters into the equations (3.36) through (3.38), the equations of motion can be written as:

$$\ddot{\gamma}_1 - (\nu + 2\omega_c + k_t\nu)\dot{\gamma}_3 + [k_t(3\omega_c^2 - \nu\omega_c) - \omega_c(\nu + \omega_c)]\gamma_1 = 0 \tag{3.41}$$

$$\ddot{\gamma}_2 = 0 \tag{3.42}$$

$$\ddot{\gamma}_3 + (\nu + 2\omega_c + k_t\nu)\dot{\gamma}_1 - [k_t\nu\omega_c + \omega_c(\nu + \omega_c)]\gamma_3 = 0 \tag{3.43}$$

These three equations now have constant coefficients. The new variables γ_1, γ_2, γ_3 can be explained as three small angles between the orbital plane F_c and a new frame F_s, which is assumed identical with orbital frame for the reference motion. Transformation between the orbital frame and the new frame, which is called stroboscopic frame by Hughes, is [17]:

$$R^{sc} = \begin{bmatrix} 1 & \gamma_3 & -\gamma_2 \\ -\gamma_3 & 1 & \gamma_1 \\ \gamma_2 & -\gamma_1 & 1 \end{bmatrix} \tag{3.44}$$

Because all perturbations occur between these two frames, transformation between the body fixed frame and stroboscopic frame is:

$$R^{bs} = R_2[(\nu + \omega_c)t] \tag{3.45}$$

It is easy to see that $R^{bs}\, R^{si}$ must be equal to $R^{ba} R^{ai}$:

$$R^{bs}\, R^{si} = R^{ba}\, R^{ai} \tag{3.46}$$

The transformation between the stroboscopic frame and the inertial frame is:

$$R^{si} = R^{sc}\, R^{ca} \tag{3.47}$$

And the transformation between reference spin frame and the inertial frame is:

$$R^{ai} = R_2(\nu t) \tag{3.48}$$

Substituting the equations (3.47) and (3.48) into the equation (3.46) gives:

$$R_2[(\nu + \omega_c)t]\, R^{sc}\, R_2(-\omega_c) = R^{ba}\, R_2(\nu t) \tag{3.49}$$

Transformation between stroboscopic frame and the orbital frame becomes:

$$R^{sc} = R_2[-(\nu + \omega_c)t]\, R^{ba}\, R_2[(\nu + \omega_c)t] \tag{3.50}$$

As a result the transformation matrix between stroboscopic frame and the orbital frame can be written as:

$$\begin{bmatrix} 1 & \gamma_3 & -\gamma_2 \\ -\gamma_3 & 1 & \gamma_1 \\ \gamma_2 & -\gamma_1 & 1 \end{bmatrix} = \begin{bmatrix} c & 0 & s \\ 0 & 1 & 0 \\ -s & 0 & c \end{bmatrix} \begin{bmatrix} 1 & \alpha_3 & -\alpha_2 \\ -\alpha_3 & 1 & \alpha_1 \\ \alpha_2 & -\alpha 1 & 1 \end{bmatrix} \begin{bmatrix} c & 0 & -s \\ 0 & 1 & 0 \\ s & 0 & c \end{bmatrix} \tag{3.51}$$

where:

$$c = \cos[(\nu + \omega_c)t] \quad \text{and} \quad s = \sin[(\nu + \omega_c t)] \tag{3.52}$$

Multiplying out equation (3.51), gives:

$$\begin{bmatrix} 1 & \gamma_3 & -\gamma_2 \\ -\gamma_3 & 1 & \gamma_1 \\ \gamma_2 & -\gamma_1 & 1 \end{bmatrix} = \begin{bmatrix} c^2 + s^2 & \alpha_3 c - \alpha_1 s & -\alpha_2 (c^2 + s^2) \\ -\alpha_3 c + \alpha_1 s & c^2 + s^2 & \alpha_3 s + \alpha_1 c \\ \alpha_2 (c^2 + s^2) & -\alpha_3 s + \alpha_1 c & c^2 + s^2 \end{bmatrix} \tag{3.53}$$

where:

$$\cos^2[(\nu + \omega_c)t] + \sin^2[(\nu + \omega_c)t] = 1 \tag{3.54}$$

Equating elements of each matrix on both side of equation (3.53) gives:

$$\begin{aligned} &(\text{i}) \quad \gamma_1(t) \triangleq \alpha_1(t)\cos(\nu + \omega_c)t + \alpha_3(t)\sin(\nu + \omega_c)t \\ &(\text{ii}) \quad \gamma_2(t) \triangleq \alpha_2(t) \\ &(\text{iii}) \quad \gamma_3(t) \triangleq -\alpha_1(t)\sin(\nu + \omega_c)t + \alpha_3(t)\cos(\nu + \omega_c)t \end{aligned} \tag{3.55}$$

which agrees with equations (3.40).

3.1.2 The Likins-Pringle Relative Equilibria

The Likins-Pringle relative equilibria extend the Thomson equilibria to the case where the spin axis is not normal to the orbital plane [17]. The term "relative equilibrium" denotes a spin axis that remains fixed with respect to the orbital frame F_c. Likins-Pringle relative equilibria allow a non zero torque unlike the Thomson equilibria, where the spin axis is normal to the orbit and the gravitational torque disappears. If the stroboscopic frame F_s is defined as the frame intermediate to the body frame F_b and the orbital frame F_c, the transformation between these frames is:

$$R^{bc} = R^{bs} R^{sc} \quad \text{and} \quad R^{bs} = R_2[(\nu + \omega_c)t] \tag{3.56}$$

In the Thomson equilibrium for the reference motion without any perturbation, R^{sc} is equal to unit matrix. For the Likins-Pringle relative equilibrium it is a constant matrix, but not equal to the unit matrix.

$$R^{sc} = R_\gamma^{sc}\, R_1(\Phi) \tag{3.57}$$

The term R_γ^{sc} indicates the small excursion angles between the stroboscopic frame and the orbital frame, and Φ is the rotation angle about the forward direction of the orbital frame $\hat{c}_1$.

The absolute angular velocity of the satellite is:

$$\overline{\omega}^{bi} = \overline{\omega}^{bs} + \overline{\omega}^{si} \tag{3.58}$$

$$\overline{\omega}^{bi} = (\nu + \omega_c)\hat{b}_2 + R^{bs}\overline{\omega}^{si} \tag{3.59}$$

The angular velocity of the satellite in stroboscopic frame is:

$$\overline{\omega}^{bi} = R_2[-(\nu + \omega_c)]\overline{\omega}^{bs} + \overline{\omega}^{si} \tag{3.60}$$

The absolute angular velocity of the stroboscopic frame F_s is:

$$\overline{\omega}^{si} = \overline{\omega}^{sc} + \overline{\omega}^{ci} \tag{3.61}$$

Equation (3.61) includes the nominal motion and the small excursion angles. The term $\overline{\omega}^{sc}$ indicates the angular velocity due to the excursion angles. For small excursion angles γ_i equation (3.61) can be approximated by:

$$\overline{\omega}^{si} = \dot{\gamma}_1 \hat{s}_1 + \dot{\gamma}_2 \hat{s}_2 + \dot{\gamma}_3 \hat{s}_3 - \omega_c \hat{c}_2 \tag{3.62}$$

The last term of the equation (3.62) can be transformed into the stroboscopic frame by using the transformation between the orbital frame F_c and the stroboscopic frame F_s as:

$$-\omega_c \hat{c}_2 = R^{sc} \begin{bmatrix} 0 \\ -\omega_c \\ 0 \end{bmatrix} = -\omega_c \, c_2^s \tag{3.63}$$

where the term c_2^s is the second column of the rotation matrix R^{sc}.

For the equilibrium condition without any perturbation:

$$\overline{\omega}^{sc} \equiv 0 \tag{3.64}$$

Therefore the absolute angular velocity of stroboscopic frame is:

$$\overline{\omega}^{si} = -\omega_c \, c_{12}^s \, \hat{s}_1 - \omega_c \, c_{22}^s \, \hat{s}_2 - \omega_c \, c_{32}^s \, \hat{s}_3 \tag{3.65}$$

where the terms c_{ij}^s indicates the elements of the rotation matrix R^{sc}.

Substituting equation (3.65) into the equation (3.60), the angular velocity of the satellite in stroboscopic frame becomes:

$$\overline{\omega}^{bi} = \omega_1 \, \hat{s}_1 + \omega_2 \, \hat{s}_2 + \omega_3 \, \hat{s}_3 \tag{3.66}$$

where the scalar terms in the equation (3.66):

$$\text{(i)} \qquad \omega_1 = -\omega_c\, c_{12}^s$$

$$\text{(ii)} \qquad \omega_2 = -\omega_c\, c_{22}^s + (\nu + \omega_c)$$

$$\text{(iii)} \qquad \omega_3 = -\omega_c\, c_{32}^s \tag{3.67}$$

To formulate the equations of motion in the stroboscopic frame F_s, gravity gradient torque in this frame can be found by the equation for the symmetrical satellite[17]:

$$\overline{M}_s = M_1\, \hat{s}_1 + M_2\, \hat{s}_2 + M_3\, \hat{s}_3 \tag{3.68}$$

$$\overline{M}_s = 3\omega_c^2 \begin{bmatrix} (I_t - I_a) c_{23}^s c_{33}^s \\ 0 \\ (I_a - I_t) c_{13}^s c_{23}^s \end{bmatrix} \tag{3.69}$$

Equations of motion become:

$$\text{(i)} \quad I_t \dot{\omega}_1^{\,bi} + (I_t - I_a)\omega_2^{bi}\omega_3^{bi} = \mathrm{M}_1$$

$$\text{(ii)} \quad I_a \dot{\omega}_2^{\,bi} + (I_t - I_t)\omega_1^{bi}\omega_3^{bi} = \mathrm{M}_2$$

$$\text{(iii)} \quad I_t \dot{\omega}_3^{bi} + (I_a - I_t)\omega_1^{bi}\omega_2^{bi} = \mathrm{M}_3 \tag{3.70}$$

Differentiation of the angular velocity can be calculated with the equation:

$$\dot{\overline{\omega}}^{bi} = \frac{^b d}{dt}\overline{\omega}^{bi} + \overline{\omega}^{si}\, x\, \overline{\omega}^{bi} \tag{3.71}$$

Thus the derivation of the angular velocity of the satellite in stroboscopic frame is:

$$\dot{\overline{\omega}}^{bi} = \omega_c\, c_{32}^s (\nu + \omega_c)\, \hat{s}_1 - \omega_c\, c_{12}^s (\nu + \omega_c)\, \hat{s}_3 \tag{3.72}$$

substituting equations (3.67), (3.69) and (3.72) into equations (3.70), the nontrivial components of the equation of motion are:

$$\begin{aligned} &(\text{i}) \quad k_t(3c_{23}^s c_{33}^s - c_{22}^s c_{32}^s) + (1+k_t)(1+\hat{\nu})c_{32}^s = 0 \\ &(\text{ii}) \quad k_t(3c_{23}^s c_{13}^s - c_{22}^s c_{12}^s) + (1+k_t)(1+\hat{\nu})c_{12}^s = 0 \end{aligned} \tag{3.73}$$

where $k_t \triangleq (I_a - I_t)/I_t$ and $\hat{\nu} \triangleq \nu/\omega_c$. These equations are satisfied in Thomson equilibrium by considering R^{sc} as a unit matrix. For the Likins-Pringle equilibrium multiply equation (3.73 i) by c_{12}^s, and (3.73 ii) by c_{32}^s and subtract to get:

$$k_t c_{23}^s (c_{32}^s c_{13}^s - c_{12}^s c_{33}^s) = 0 \tag{3.74}$$

By using the relationships between the elements of R^{sc} the expression in the parentheses is equal to c_{21}^s (Appendix B). So the final form of the equilibrium conditions shows that there are two types of Likins-Pringle equilibria conditions:

$$\begin{aligned} &(\text{i}) \quad c_{23}^s = 0 \; ; \quad c_{21}^s \neq 0 \\ &(\text{ii}) \quad c_{23}^s \neq 0 \; ; \quad c_{21}^s = 0 \end{aligned} \tag{3.75}$$

For the equation (3.75 i) the spin axis $\hat{p}_2$ is normal to the vertical axis of the orbit frame $\hat{c}_3$, but not normal to the forward direction of the orbit frame $\hat{c}_1$, so the spin axis generates a hyperboloid in inertial space (Figure 3.3). However this condition is not the interest of this study. On the other hand the equation (3.75 ii) implies that the spin axis is normal to the forward direction but not to the vertical, and the spin axis produces a cone in inertial space. The results for conical case can be obtained by solving equations (3.73i) and (3.73 ii) for $c_{23}^s \neq 0$ and $c_{21}^s = 0$.

From Appendix B:

(i) $c_{33}^s = c_{11}^s c_{22}^s - c_{12}^s c_{21}^s \quad \Rightarrow \quad c_{33}^s = c_{11}^s c_{22}^s$ since $c_{21}^s = 0$

(ii) $c_{32}^s = c_{13}^s c_{21}^s - c_{11}^s c_{23}^s \quad \Rightarrow \quad c_{32}^s = -c_{11}^s c_{23}^s$ since $c_{21}^s = 0$ then

$$c_{23}^s = -\frac{c_{32}^s}{c_{11}^s} \tag{3.76}$$

Substituting (3.76 i) and (3.76 ii) into (3.73 i) yields:

$$k_t(3(-\frac{c_{32}^s}{c_{11}^s})(c_{11}^s c_{22}^s) - c_{22}^s c_{32}^s) + (1+k_t)(1+\hat{\nu})c_{32}^s = 0$$

$$k_t(-4c_{22}^s c_{32}^s) + (1+k_t)(1+\hat{\nu})c_{32}^s = 0 \tag{3.77}$$

From Appendix B:

(i) $c_{13}^s = c_{21}^s c_{32}^s - c_{22}^s c_{31}^s \quad \Rightarrow \quad c_{13}^s = -c_{22}^s c_{31}^s$ since $c_{21}^s = 0$

(ii) $c_{12}^s = c_{23}^s c_{31}^s - c_{21}^s c_{33}^s \quad \Rightarrow \quad c_{12}^s = c_{23}^s c_{31}^s$ since $c_{21}^s = 0$ then

$$c_{23}^s = \frac{c_{12}^s}{c_{31}^s} \tag{3.78}$$

Substituting (3.78 i) and (3.78 ii) into the equation (3.73 ii) yields:

$$k_t(3\frac{c_{12}^s}{c_{31}^s}(-c_{22}^s c_{31}^s) - c_{22}^s c_{12}^s) + (1+k_t)(1+\hat{\nu})c_{12}^s = 0$$

$$k_t(-4c_{22}^s c_{12}^s) + (1+k_t)(1+\hat{\nu})c_{12}^s = 0 \tag{3.79}$$

As a result, equations (3.77) and (3.79) become:

(i) $c_{32}^s[-4k_t c_{22}^s + (1+k_t)(1+\hat{\nu})] = 0$

(ii) $c_{12}^s[-4k_t c_{22}^s + (1+k_t)(1+\hat{\nu})] = 0 \tag{3.80}$

Since c_{23}^{s} would be zero when both c_{12}^{s} and c_{32}^{s} are zero, these equations can only be satisfied when the expression in the parenthesis is zero. The solution for these equations is given by:

$$c_{21}^{s} = 0 \qquad c_{22}^{s} = \cos\Phi \hat{=} \frac{(1+k_t)(1+\hat{\nu})}{4k_t} \tag{3.81}$$

where Φ is the constant rotation angle about the forward axis of the orbit frame.

The transformation between the stroboscopic frame F_s and the orbital frame F_c is:

$$R^{sc} = R_{\gamma}\, R_1(\Phi) \tag{3.82}$$

where Φ is the constant tilt of the spin axis about the forward direction of the orbit frame and γ represents the three small angles which allow small attitude excursions about the nominal motion. Therefore the transformation matrix between the stroboscopic frame and the orbital frame is:

$$R^{sc} = \begin{bmatrix} 1 & \gamma_3 & -\gamma_2 \\ -\gamma_3 & 1 & \gamma_1 \\ \gamma_2 & -\gamma_1 & 1 \end{bmatrix} \begin{bmatrix} 1 & 0 & 0 \\ 0 & \cos\Phi & \sin\Phi \\ 0 & -\sin\Phi & \cos\Phi \end{bmatrix} \tag{3.83}$$

By using these relationships, the linearized equations of motion are given by Hughes as [17]:

$$\text{(i)} \quad \ddot{\gamma}_1 - (1+k_t)(\omega \sin\Phi)\dot{\gamma}_2 - (1+3k_t)(\omega_c \cos\Phi)\dot{\gamma}_3 - 4k_t(\omega_c \sin\Phi)^2 \gamma_1 = 0$$

$$\text{(ii)} \quad \ddot{\gamma}_2 + (\omega_c \sin\Phi)\dot{\gamma}_1 = 0$$

$$\text{(iii)} \quad \ddot{\gamma}_3 + (1+3k_t)(\omega \cos\Phi)\dot{\gamma}_1 - 3k_t\omega_c^2\gamma_3 = 0 \tag{3.84}$$

Because it is impossible to maintain the stability for the spin rate of spinning satellite, this research is only concerned with the stability of the spin axis (i.e. γ_1 and γ_3). After integrating the second equation and substitution in the first equation, new equations for the angles γ_1 and γ_3 can be found [17].

$$\text{(i)} \quad \ddot{\gamma}_1 - (1+3k_t)(\omega_c \cos\Phi)\dot{\gamma}_3 + (1-3k_t)(\omega_c \sin\Phi)^2 \gamma_1 = 0$$

$$\text{(ii)} \quad \ddot{\gamma}_3 + (1+3k_t)(\omega_c \cos\Phi)\dot{\gamma}_1 - 3k_t\omega_c^2\gamma_3 = 0 \tag{3.85}$$

The characteristic equations for these two equations are:

$$\left(\frac{s}{\omega_c}\right)^4 + b_1\left(\frac{s}{\omega_c}\right)^2 + b_2 = 0 \tag{3.86}$$

$$b_1 = 1 + 3k_t + 9k_t^2 - 9k_t(1+kt)\sin^2\Phi \tag{3.87}$$

$$b_2 = -3k_t(1-3k_t)\sin^2\Phi \tag{3.88}$$

The necessary and sufficient conditions for infinitesimal stability are:

$b_1 > 0$

$b_2 > 0$

$b_1^2 - 4b_2 > 0$

The regions in which these conditions are satisfied are shown in Figure 3.5. The initial design of the TSS will be based on these stable regions from the rigid body analysis.

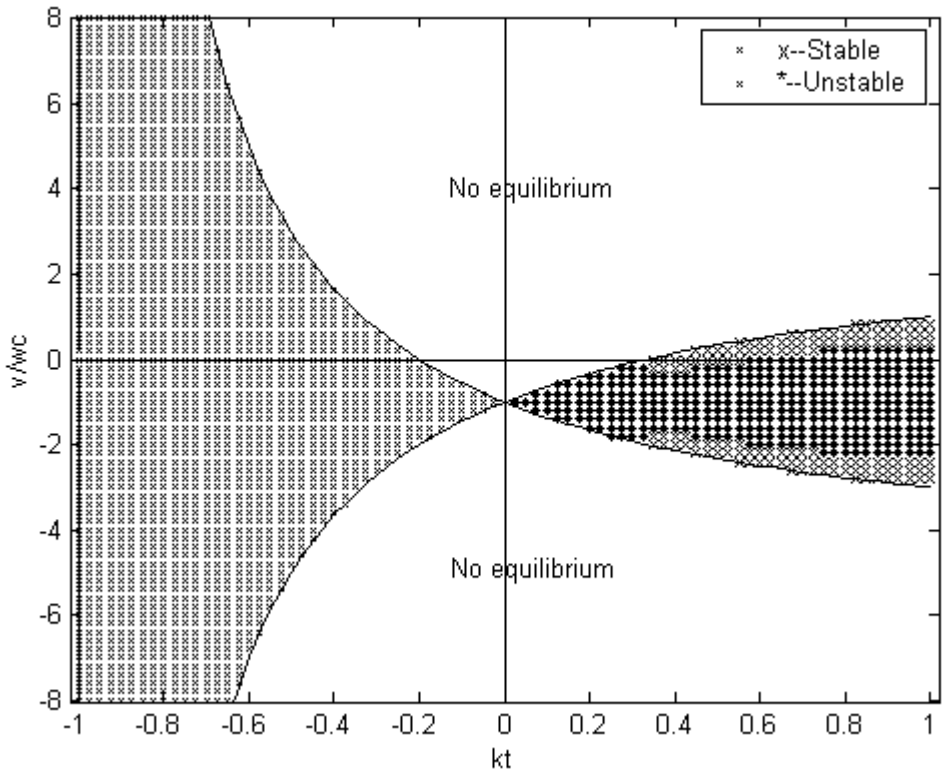

Figure 3.5 Stability Diagram for the Likins-Pringle Equilibria [17]

3.2 Design of a Tethered Satellite System

The tethered satellite system which is the subject of this thesis consists of three satellites at the corners of an equilateral triangle with the same mass, and two end bodies at the opposite sides of this triangular plane. Satellites and end bodies masses are considered as point masses. The tethered satellite system is shown in Figure 3.6

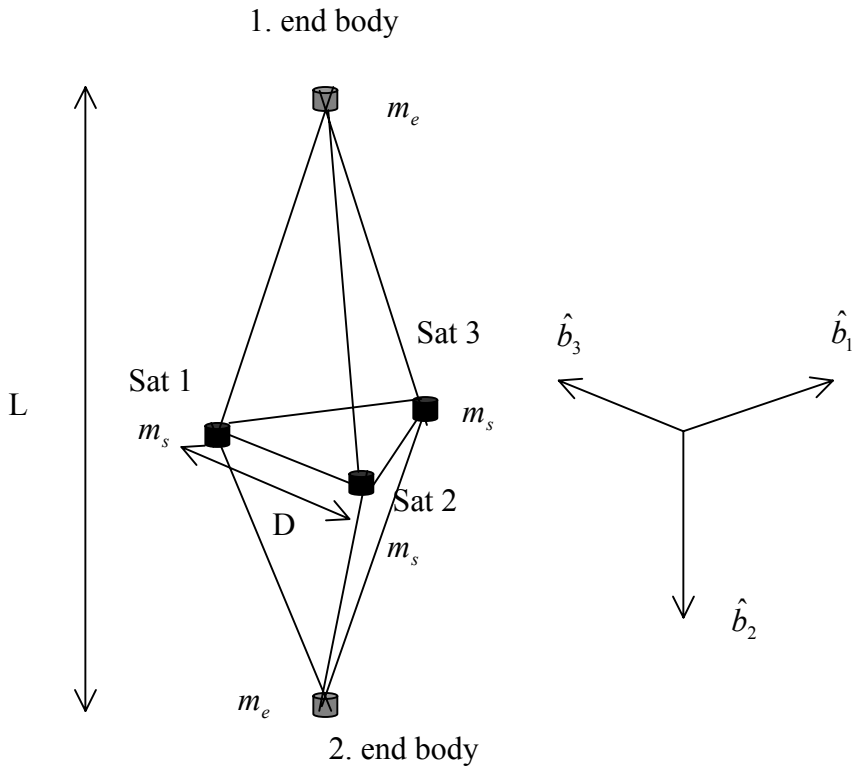

Figure 3.6 Design Of The tethered Satellite System

In Figure 3.6 mass of the satellites are given by m_s and the mass of the end bodies are given by the term m_e. D gives the distance between the satellites in equilateral plane, and L is the distance between the two end bodies. Because of the axisymmetry of the

formation, the center of mass of the system is on the triangular plane and at the center of the this triangular plane. Position of the satellites and the end bodies with respect to the center of mass of the system are:

$$
\begin{aligned}
&(\text{a}) \quad \bar{r}_{e1}^{b} = \begin{bmatrix} 0 & -L/2 & 0 \end{bmatrix} \\
&(\text{b}) \quad \bar{r}_{e2}^{b} = \begin{bmatrix} 0 & L/2 & 0 \end{bmatrix} \\
&(\text{c}) \quad \bar{r}_{s1}^{b} = \begin{bmatrix} -D/2 & 0 & D/(2\sqrt{3}) \end{bmatrix} \\
&(\text{d}) \quad \bar{r}_{s2}^{b} = \begin{bmatrix} 0 & 0 & -D/\sqrt{3} \end{bmatrix} \\
&(\text{e}) \quad \bar{r}_{s3}^{b} = \begin{bmatrix} D/2 & 0 & D/(2\sqrt{3}) \end{bmatrix}
\end{aligned} \tag{3.89}
$$

and the total inertias of the system is:

$$
I = I_{e1} + I_{e2} + I_{s1} + I_{s2} + I_{s3} \tag{3.90}
$$

where the terms I_{e1} and I_{e2} are the inertias of the end bodies, and the terms I_{s1}, I_{s2}, and I_{s3} indicate the inertias of the satellites

$$
I = \begin{bmatrix} \dfrac{m_e L^2}{2} + \dfrac{D^2 m_s}{2} & 0 & 0 \\ 0 & D^2 m_s & 0 \\ 0 & 0 & \dfrac{m_e L^2}{2} + \dfrac{D^2 m_s}{2} \end{bmatrix} = \begin{bmatrix} I_t & 0 & 0 \\ 0 & I_a & 0 \\ 0 & 0 & I_t \end{bmatrix} \tag{3.91}
$$

where the axial and transverse inertias are I_a and I_t respectively. The variable k_t is defined as:

$$
k_t = \frac{I_a - I_t}{I_t} \tag{3.92}
$$

Substituting in the inertias for the TSS yields:

$$k_t == \frac{d^2 m_s - \left(\frac{m_e L^2}{2} + \frac{d^2 m_s}{2} \right)}{\frac{m_e L^2}{2} + \frac{d^2 m_s}{2}} \tag{3.93}$$

To analyze the parameter k_t, it is possible to define non-dimensional variables:

$$\hat{d} = \frac{D}{L} \qquad \text{and} \qquad \hat{m} = \frac{m_s}{m_e} \tag{3.94}$$

Therefore equation (3.93), can be expressed as:

$$k_t = \frac{\hat{m}\hat{d}^2 - 1}{\hat{m}\hat{d}^2 + 1} \tag{3.95}$$

Figure shows the k_t parameters for different values of $\hat{d}$ and $\hat{m}$ parameters.

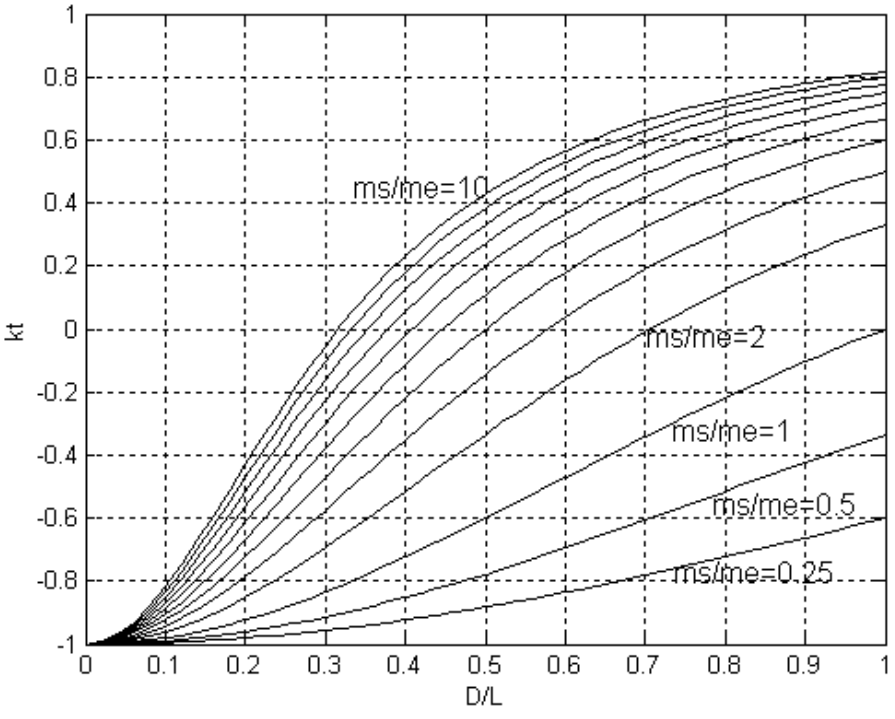

Figure 3.7 k_t Values for Mass and Size Ratios

The Likins-Pringle relative equilibria states that there is a constant rotation angle about the forward direction ($\hat{c}_1$) of the orbit. The spin axis of the satellite generates a cone in inertial space [17], and the rotation angle about the forward direction gives the half cone angle. The equation for the half cone angle is:

$$c_{22}^{s} = \cos\Phi \triangleq \frac{(1+k_t)(1+\hat{\nu})}{4k_t} \tag{3.96}$$

where: $$k_t = \frac{I_a - I_t}{I_t} \qquad \text{and} \qquad \hat{\nu} = \frac{\nu}{\omega_c} \tag{3.97}$$

Reference frames for this orientation and the half cone angle is shown in Figure 3.8. Note that the spin axis of the formation is $\hat{s}_2$, so a half cone angle of 90^o implies the formation is aligned with the local vertical.

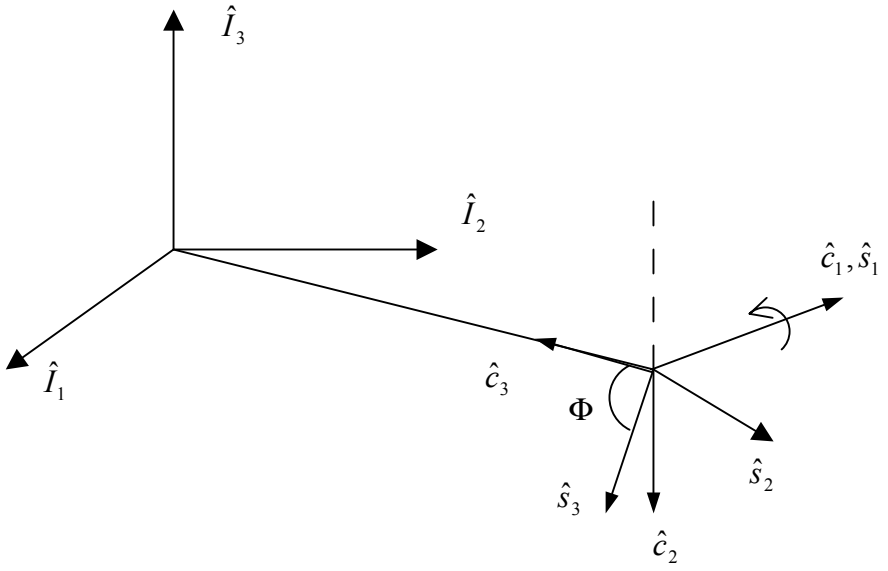

Figure 3.8 Reference Frames

To analyze the effects of the spin rate and the distance parameters of the TSS design on the equilibrium position of the formation, equation (3.96) can be used. Figure 3.8 shows the half-cone angle for different L/D and spin ratios with constant mass ratio of $m_s / m_e = 2$.

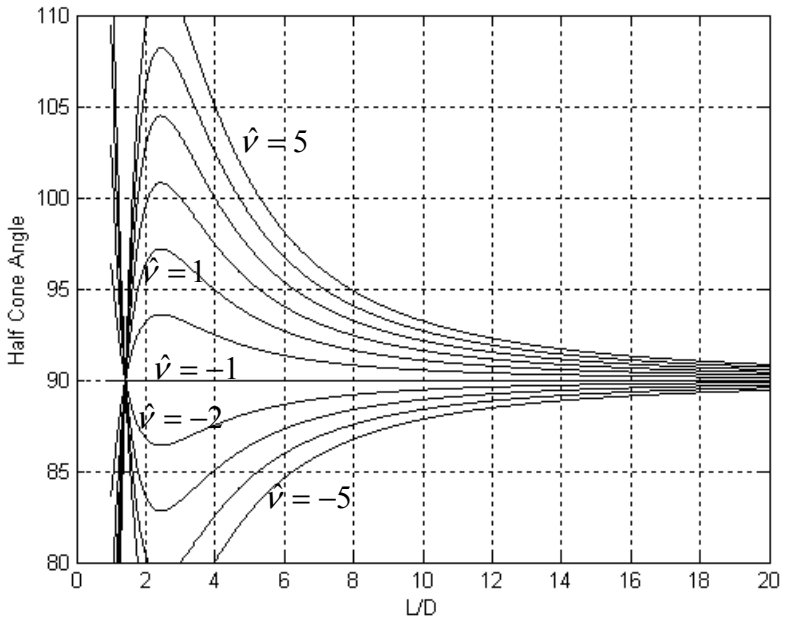

Figure 3.9 Half-Cone Angle for Different Spin Rates

In Figure 3.9 the half cone angle increases with increasing positive spin rate $\hat{\nu}$ or decreasing size ratio L / D. To obtain the equilibrium position of the tethered formation at nadir direction the half-cone angle should be 90^0 deg, which is achievable with the spin rate:

$$\hat{\nu} = -1 \tag{3.97}$$

According to equation (3.56), this spin rate implies that the satellite doesn't spin about its symmetry axis with respect to the stroboscopic frame. However a tethered satellite system, which consists of distributed satellites must rotate about the symmetry axis to rigidize the system and to obtain the stability. The spin rate about the symmetry axis of the tethered formation with respect to the stroboscopic frame is:

$$\hat{\nu}_s \triangleq \frac{\nu + \omega_c}{\omega_c} \tag{3.98}$$

Substituting $\hat{\nu}$ into the equation (3.98) yields:

$$\hat{\nu}_s \triangleq \hat{\nu} + 1 \tag{3.99}$$

By using this relationship it can be seen that there is symmetry in the Figure 3.8 for the:

$$\hat{\nu}_s = 0 \tag{3.100}$$

This result implies that positive spin rates about the symmetry axis $\hat{b}_2$ in the body frame gives the half-cone angle greater than 90^0 degree and negative spin rates about the symmetry axis $\hat{b}_2$ in the body frame gives the half-cone angle less than 90^0 degree.

The other way to get a half-cone angle closer to 90 degree is to increase the size ratio of formation, which is denoted by L/D in Figure 3.9. Increasing the distance between the two end bodies increases the ratio L/D and causes to the half-cone angle to approach 90^o, which implies the spin axis is on the nadir direction.

To analyze the effects of all parameters of the TSS design, (spin rate, mass ratio and the size ratio) on the equilibrium position of the formation on the orbit, non–dimensional variables in equation 3.94 and equation 3.95 can be used. By using the non-

dimensional variables k_t and the spin rate $\hat{\nu}$, the rotation angle about the forward orbit direction is shown in Figure 3.10.

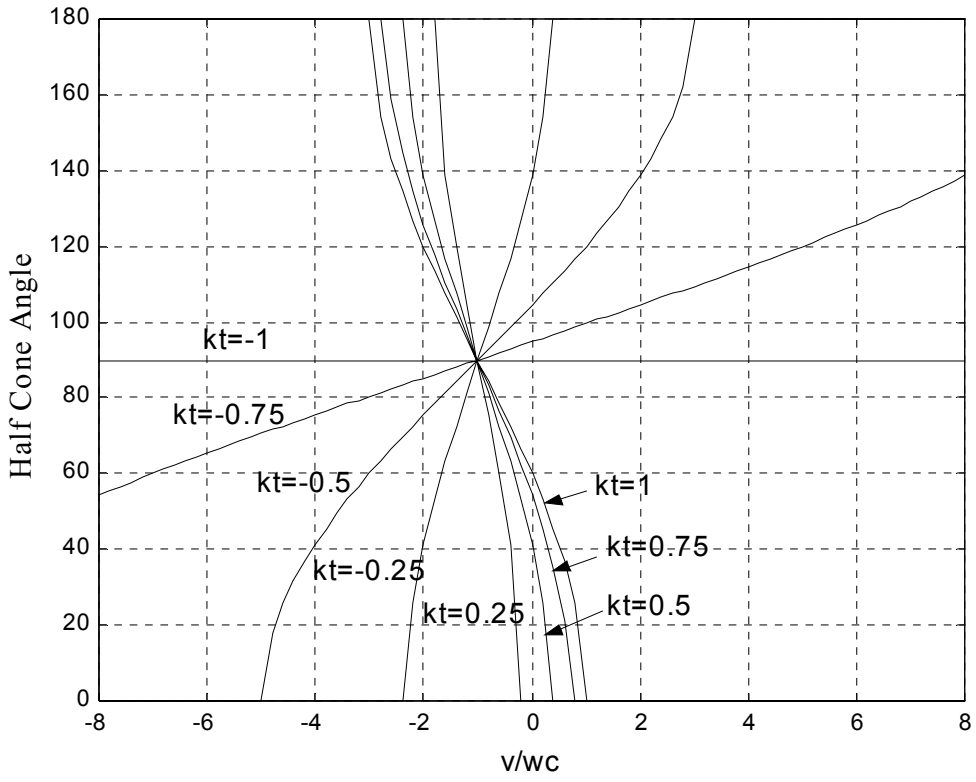

Figure 3.10 Half-Cone Angle for Conical Stability

For the Figure 3.10 there is symmetry for the half cone angle about the spin rate:

$$\hat{\nu} = -1 \tag{3.101}$$

As with the analysis before, this implies that the satellite does not spin with respect to the stroboscopic frame. To design a tethered formation in the stability region, which has the spin axis closer to the nadir direction, the spin rate should be as small as possible and the variable k_t must be negative and close to –1.

IV. Analysis and Results

To analyze the dynamics of the tethered satellite system, equations of motion for each satellite are developed and solved numerically. In this chapter, forces on the satellites and the end bodies will be determined. In this study, perturbation forces like earth oblateness, gravity effect of sun or the gravity effect of moon are not considered.

To keep the tethered satellites at the desired positions with respect to the each other, the system must rotate at some minimum rate. Parameters that affect the minimum spin rate will be explained below.

Numerical solutions for the equations of motion will be explained using the Likins-Pringle equilibria. The stability region will be presented where the tethered satellite system is stable (by the definition of the stability used for this study). Specific examples in this region will be explained in more detail. Stability of the systems for these examples will be discussed and the parameters which have effects on the stability of the systems will be explained.

4.1. Equations of Motion

The equation of motion for a satellite in a inverse square gravity field is [19]:

$$m\ddot{\bar{r}} = -\frac{\mu m}{|\bar{r}|^3}\bar{r} \tag{4.1}$$

where μ is the earth gravitational parameters, m is the mass of the satellite and $\bar{r}$ denotes the position of the satellite from the center of the earth. However, due to the perturbing forces transmitted to the satellites through the tethers, the motion of each satellite in a tethered system is non-Keplerian. For a simple tethered satellite system, where the tether is considered as a massless and extensible string, forces on the particles can be shown in Figure 4.1 [18].

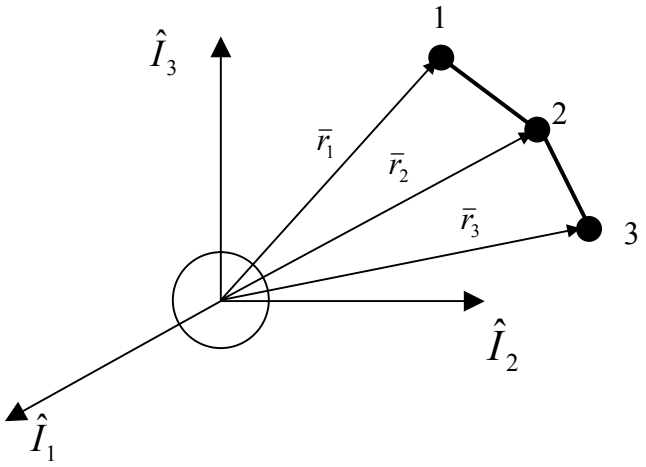

Figure 4.1 Three Satellites With Tethers

Three satellites, which are connected to each other with tethers are shown in Figure 4.1. Their distances from the center of the earth are presented with $\bar{r}_i$ vectors. There are two types of forces on each satellite, which are the gravitational force and the tension force. Gravitational force depends on the distance of satellite from the center of the earth, and tension force depends on the distance between satellites and the tether length. Equations of motion for each satellite are:

$$m_1 \ddot{\bar{r}}_1 = -\frac{\mu m_1}{|\bar{r}_1|^3}\bar{r}_1 + T_{12}\frac{\bar{r}_{12}}{|\bar{r}_{12}|} \tag{4.2}$$

$$m_2 \ddot{\bar{r}}_2 = -\frac{\mu m_2}{|\bar{r}_2|^3}\bar{r}_2 - T_{12}\frac{\bar{r}_{12}}{|\bar{r}_{12}|} - T_{23}\frac{\bar{r}_{32}}{|\bar{r}_{32}|} \tag{4.3}$$

$$m_3 \ddot{\bar{r}}_3 = -\frac{\mu m_3}{|\bar{r}_3|^3}\bar{r}_3 + T_{23}\frac{\bar{r}_{32}}{|\bar{r}_{32}|} \tag{4.4}$$

where m_i is the mass of the satellite and, T_{ij} is the tension force between bodies i and j and:

$$\bar{r}_{12} = \bar{r}_2 - \bar{r}_1 \quad \text{and} \quad \bar{r}_{32} = \bar{r}_2 - \bar{r}_3 \tag{4.5}$$

The $\frac{\bar{r}_{ij}}{|\bar{r}_{ij}|}$ terms show the direction of the tension force.

Magnitude of the tension force can be given by [7]:

$$T_{ij} = \begin{cases} E\left(|\bar{r}_i - \bar{r}_j| - l_{ij}\right) & if \quad l_{ij} < |\bar{r}_i - \bar{r}_j| \\ 0 & if \quad l_{ij} > |\bar{r}_i - \bar{r}_j| \end{cases} \tag{4.6}$$

where E is the tether extension stiffness and l_{ij} is the unstretched tether length. It is obvious that the tension force occurs only when the distance between the satellites is greater than its initial value and there is no compressive force.

With these basic equations, equations of motion for the Tethered Satellite System model, which consists of three satellites at the corners of an equilateral triangle and two end bodies at opposite side of this plane, connected with massless and elastic tether to each other can be presented. Figure 4.2 shows the orientation of the tethered satellite system on orbit.

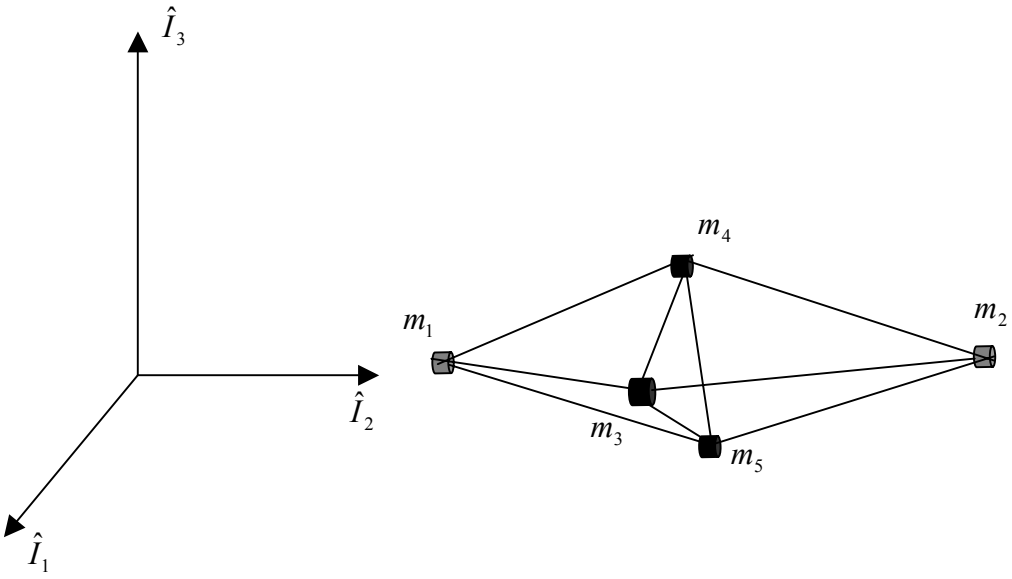

Figure 4.2 Orientation of TSS on Orbit

$$m_1\ddot{\bar{r}}_1 = -\frac{\mu m_1}{|\bar{r}_1|^3}\bar{r}_1 - T_{13}\frac{\bar{r}_{13}}{|\bar{r}_{13}|} - T_{14}\frac{\bar{r}_{14}}{|\bar{r}_{14}|} - T_{15}\frac{\bar{r}_{15}}{|\bar{r}_{15}|} \tag{4.7}$$

$$m_2\ddot{\bar{r}}_2 = -\frac{\mu m_2}{|\bar{r}_2|^3}\bar{r}_2 - T_{23}\frac{\bar{r}_{23}}{|\bar{r}_{23}|} - T_{24}\frac{\bar{r}_{24}}{|\bar{r}_{24}|} - T_{25}\frac{\bar{r}_{25}}{|\bar{r}_{25}|} \tag{4.8}$$

$$m_3\ddot{\bar{r}}_3 = -\frac{\mu m_3}{|\bar{r}_3|^3}\bar{r}_3 + T_{13}\frac{\bar{r}_{13}}{|\bar{r}_{13}|} + T_{23}\frac{\bar{r}_{23}}{|\bar{r}_{23}|} - T_{34}\frac{\bar{r}_{34}}{|\bar{r}_{34}|} - T_{35}\frac{\bar{r}_{35}}{|\bar{r}_{35}|} \tag{4.9}$$

$$m_4\ddot{\bar{r}}_4 = -\frac{\mu m_4}{|\bar{r}_4|^3}\bar{r}_4 + T_{14}\frac{\bar{r}_{14}}{|\bar{r}_{14}|} + T_{24}\frac{\bar{r}_{24}}{|\bar{r}_{24}|} + T_{34}\frac{\bar{r}_{34}}{|\bar{r}_{34}|} - T_{45}\frac{\bar{r}_{45}}{|\bar{r}_{45}|} \tag{4.10}$$

$$m_5\ddot{\bar{r}}_5 = -\frac{\mu m_5}{|\bar{r}_5|^3}\bar{r}_5 + T_{15}\frac{\bar{r}_{15}}{|\bar{r}_{15}|} + T_{25}\frac{\bar{r}_{25}}{|\bar{r}_{25}|} + T_{35}\frac{\bar{r}_{35}}{|\bar{r}_{35}|} + T_{45}\frac{\bar{r}_{45}}{|\bar{r}_{45}|} \tag{4.11}$$

4.2 Minimum Spin Rate For Stability

For a rigid satellite formation system, rotation of the system can be used for attitude control. On the other hand, the tethered satellite system with flexible tethers must rotate to keep the satellites in the formation at their nominal position with respect to each other. The TSS considered for this study consists of three satellites and two end bodies. The three satellites are placed on a triangular plane. With some simple analysis it is possible to determine the minimum spin rate to keep the formation from collapsing.

The aim here is to keep the triangular plane of three satellites perpendicular to the nadir direction as much as possible. It is not possible to keep the satellites on a planar shape with a definite distance to each other without spinning. Minimum spin rate for the tethered satellite system can be found by assuming the spin axis of the tethered system is aligned with the nadir direction.

For the TSS model, the angular velocity of the system normal to the orbital plane can be calculated from the orbital mean motion:

$$\omega_c = \sqrt{\frac{\mu}{r^3}} \tag{4.12}$$

The centrifugal force is:

$$F_c = mr\omega_c^2 \tag{4.13}$$

Thus for the TSS model the net force on the end bodies in the formation is:

$$F_{net} = F_g + F_c \tag{4.14}$$

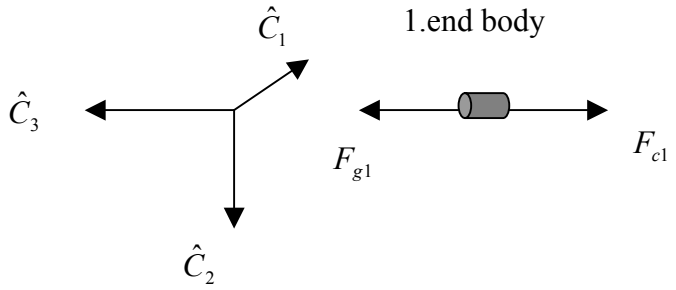

Figure 4.3 External Forces on the first end body

External forces on the first end body are presented in Figure 4.3, and by using the distance of the end body from the center of the earth:

$$\bar{r}_{1eb} = (r_{cm} - L/2)\,\hat{c}_3 \tag{4.15}$$

where r_{cm} denotes the distance of the center of mass of the system from the center of the earth. Gravitational force on the first end body is:

$$F_{g1} = -\frac{\mu m_e}{\left|\bar{r}_{eb1}\right|^3}\bar{r}_{eb1} \tag{4.16}$$

where m_e is the mass of the end body.

Substitute the equation (4.15) into the equation (4.16):

$$\overline{F}_{g1} = -\frac{\mu m_e}{\left|(r_{cm} - L/2)\right|^3}(r_{cm} - L/2)\hat{c}_3 \tag{4.17}$$

The centrifugal force on the particle is:

$$\overline{F}_{c1e} = m_e \bar{r}_{eb1}\,\omega_c^2 \tag{4.18}$$

Substituting the equations (4.12) and (4.15) into the equation (4.18) the centrifugal force on the end body is:

$$\overline{F}_{c1e} = m_e (r_{cm} - L/2) \ \frac{\mu}{r_{cm}^3} \hat{c}_3 \tag{4.20}$$

Thus the net external force is:

$$\overline{F}_{net1} = -\frac{\mu m_e}{\left|(r_{cm} - L/2)\right|^3}(r_{cm} - L/2)\hat{c}_3 + m_e (r_{cm} - L/2)\frac{\mu}{r_{cm}^3}\hat{c}_3 \tag{4.21}$$

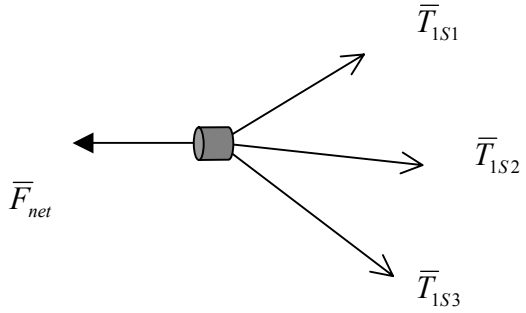

Figure 4.4 Net Forces on The End Body

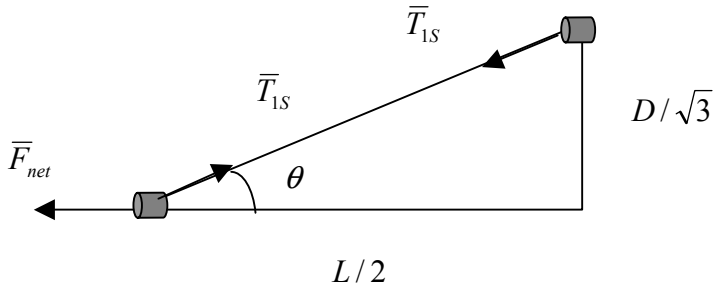

Figure 4.5 Tension Force On A Tether

The total force on the first end body and the tension force on the tether are presented in Figure 4.4 and Figure 4.5. For these figures $\overline{T}_{1si}$ denotes the tension force between the first end body and the satellite. L is the distance of the end body from the center of the mass of the system and D is the distance of the satellites from the center of mass. The angle between the symmetry axis and the tether is:

$$\theta = \arctan \frac{D/\sqrt{3}}{L/2} \tag{4.22}$$

Because of the axisymmetry of the TSS model tension force on the tethers attached to the end body are approximately equal to each other in magnitude, so:

$$\overline{F}_{net1} \frac{1}{3} = \overline{T}_{1si} \cos\theta \tag{4.23}$$

Thus the tension force on the tether is:

$$\overline{T}_{1si} = \frac{\overline{F}_{net1}}{3} \frac{1}{\cos\theta} \tag{4.24}$$

where $\overline{T}_{1si}$ denotes the tension force on the tether between the first end body and the i th satellite.

By using the same method for the second end body, which is at the opposite side of the triangular plane, the total force can be calculated. Position of the second end body is:

$$\bar{r}_{2eb} = (r_{cm} + L/2)\hat{c}_3 \tag{4.25}$$

Gravitational force on the first end body is:

$$F_{g2} = -\frac{\mu m_e}{|\bar{r}_{eb2}|^3} \bar{r}_{eb2} \tag{4.26}$$

Substituting the equation (4.25) into the equation (4.26):

$$\overline{F}_{g2} = -\frac{\mu m_e}{\left|(r_{cm} + L/2)\right|^3}(r_{cm} + L/2)\hat{c}_3 \tag{4.27}$$

The centrifugal force on the particle is:

$$\overline{F}_{c2e} = m_e \bar{r}_{eb2}\ \omega_c^2 \tag{4.28}$$

Substituting equations (4.12) and (4.25) into equation (4.28) the centrifugal force on the end body is:

$$\overline{F}_{c1e} = m_e (r_{cm} + L/2)\ \frac{\mu}{r_{cm}^3}\ \hat{c}_3 \tag{4.29}$$

Thus the net external force is:

$$\overline{F}_{net2} = -\frac{\mu m_e}{\left|(r_{cm} + L/2)\right|^3}(r_{cm} + L/2)\hat{c}_3 + m_e (r_{cm} + L/2)\ \frac{\mu}{r_{cm}^3}\hat{c}_3 \tag{4.30}$$

the geometry is similar to the first end body, so the tension force on the tethers between the second end body and the satellites are:

$$\overline{T}_{2si} = \frac{\overline{F}_{net2}}{3}\frac{1}{\cos\theta} \tag{4.31}$$

The forces on the satellites, which are placed on the equilateral triangular plane, are the tether tension forces, the centrifugal force due to the spinning of the formation, and the gravitational force.

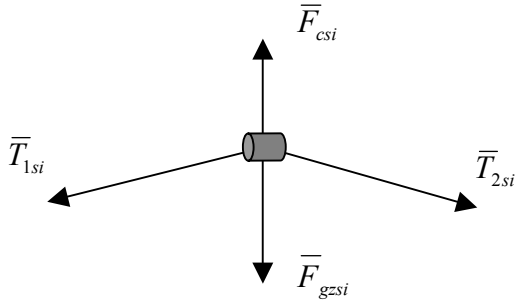

Figure 4.6 Forces On The Satellites

Where $\overline{T}_{1si}$ and $\overline{T}_{2si}$ denote the tension forces, $\overline{F}_{gzsi}$ denotes the component of the gravitational force in z direction and $\overline{F}_{csi}$ denotes the centrifugal force on the satellites. Here $\overline{F}_{csi}$ is the centrifugal force due to the spinning of the satellite. The component of the angular velocity due to the rotation of the formation around the earth is not included in this analysis since it will vary depending upon the location of the satellites.

The total force on the satellite is:

$$\overline{F}_{tot} = \overline{F}_{gzsi} + \overline{T}_{1si} + \overline{T}_{2si} + \overline{F}_{csi} \tag{4.32}$$

The centrifugal force on the satellites due to the spinning around the axis perpendicular to the triangular plane is:

$$\overline{F}_{csi} = m_s \frac{D}{\sqrt{3}} \nu_s^2 \tag{4.33}$$

where the term ν_s denotes the spin rate about the axis perpendicular to the plane with respect to the stroboscopic frame, and m_s is the mass of the satellites.

$$\nu_s = \nu + \omega_c \tag{4.34}$$

To get the equilibrium spin rate, set $\overline{F}_{tot}$ in equation (4.32) equal to zero and solve for ν_s:

$$\nu_s = \frac{\sqrt{3}}{m_s D}\left(\overline{F}_{gzi} + \overline{T}_{1si} + \overline{T}_{2si}\right) \tag{4.35}$$

This is the minimum spin rate to keep the tethers in tension. Figure 4.7 shows the values of the ν_s for a range of L/D and m_e / m_s.

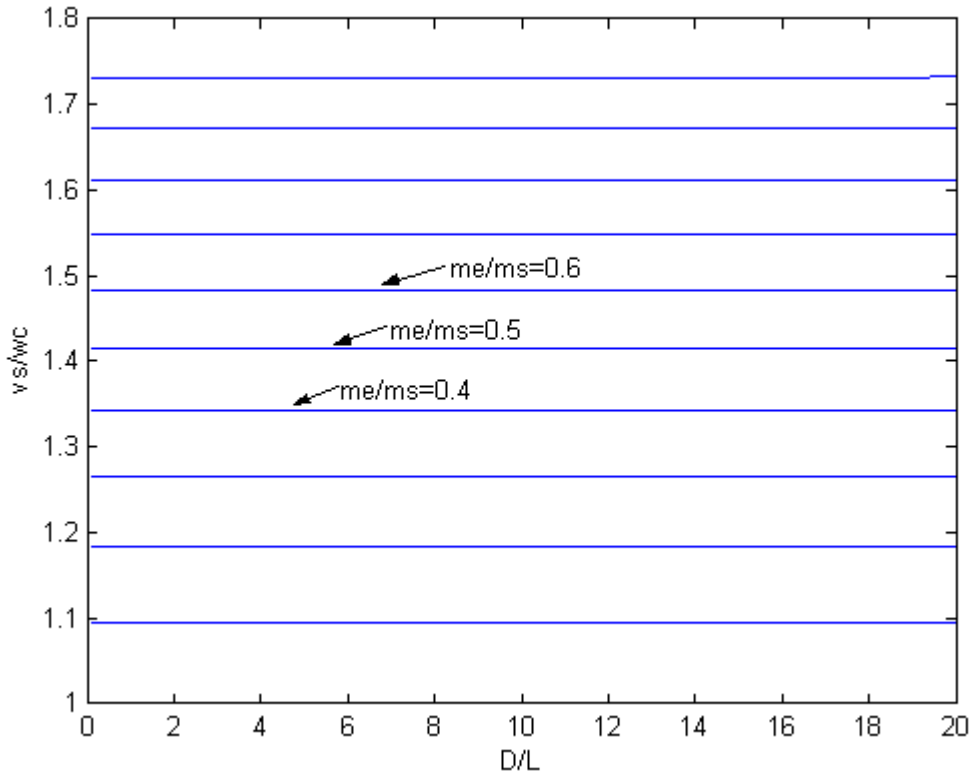

Figure 4.7 Minimum Spin Rate For Stability

Figure 4.7 shows that the minimum spin rate increases with the mass ratio, which is the ratio of the mass of the end body to the mass of the satellite for this figure. Also, the minimum spin rate doesn't depend on the distance between the end bodies. For the mass ratio 0.5 the minimum spin rate is approximately the $\sqrt{2}$ times greater than the nominal motion ω_c.

4.3 Simulation Results

The possibility of using Likins-Pringle relative equilibria for the design of the tethered satellite formation is demonstrated using numerical simulation. The equations of motion have been solved numerically because of their complexity.

The example provided here is a tethered satellite formation in a circular orbit with a radius of 8000 km. The formation is shown in Figure 4.8. Tether extension stiffness is assumed as 10^5 and constant for all simulations.

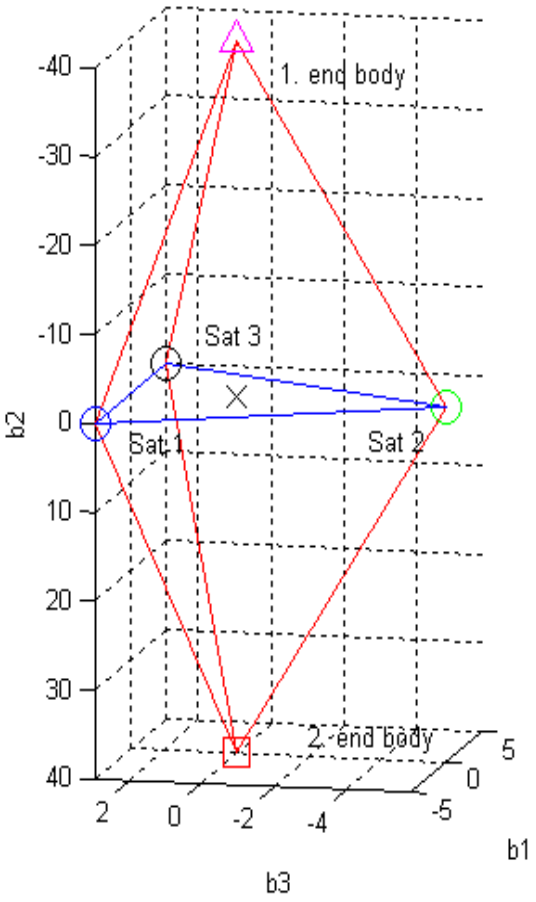

Figure 4.8 Reference Tethered Formation in the Body Frame

The formations parameters are:

$m_{sat1} = m_{sat2} = m_{sat3} = m_s = 200\,kg$ (Mass of the satellites)

$m_{ebod1} = m_{ebody2} = m_e = 100\,kg$ (Mass of the end bodies)

$L = 80\,km$ (distance between two end bodies)

$D = 10\,km$ (distance between satellites)

$\omega_c = \sqrt{\frac{\mu}{r_{cm}^3}}$ (nominal motion of the tethered formation)

$\nu_s = -2 * \omega_c$ (spin rate with respect to the stroboscopic frame)

Transverse and axial inertias of the formation are:

$$I_t = \frac{m_e L^2}{2} + \frac{D^2 m_s}{2} = 330{,}000 \tag{4.36}$$

$$I_a = D^2 m_s = 20{,}000 \tag{4.37}$$

Substituting the spin rate ν_s into equation (4.34):

$$\nu = \nu_s - \omega_c = -3 * \omega_c \tag{4.38}$$

Then the spin ratio is:

$$\hat{\nu} = \frac{\nu}{\omega_c} = -3 \tag{4.39}$$

The inertia ratio k_t is:

$$k_t = \frac{I_a - I_t}{I_t} = -0.9394 \tag{4.40}$$

For the equilibrium position of the tethered formation the half cone angle is:

$$\Phi = \arccos\left(\frac{(1+k_t)(1+\hat{\nu})}{4k_t}\right) = 88.1514 \text{ deg} \tag{4.41}$$

The angle between the spin axis and the nadir direction is:

$$90 - \Phi = 1.8486$$

Figure 4.9 shows the orientation of the reference tethered formation in the orbital frame with an angle of 1.8486 degree between the spin axis and the nadir direction.

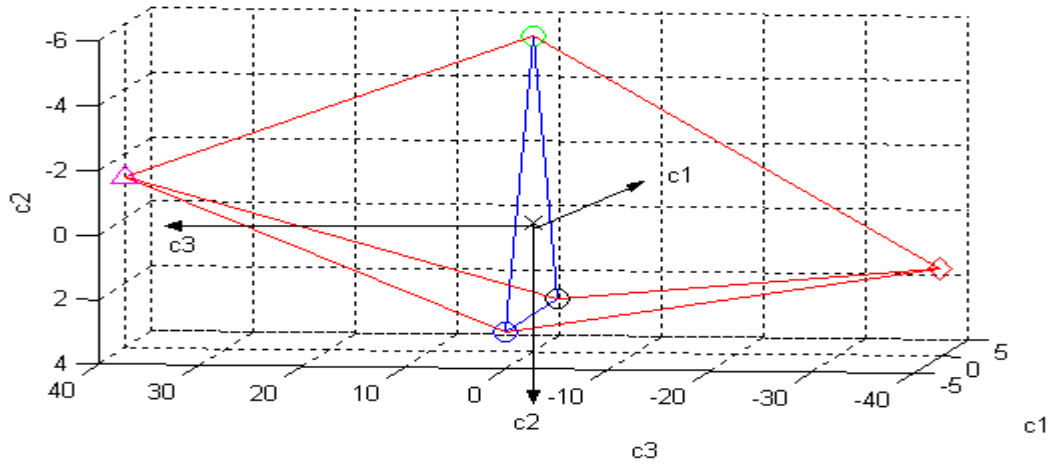

Figure 4.9 Tethered formation on the Orbital frame

With this orientation the satellites follow a circular path because of the formation spin, and the projection of the satellites on the Earth surface will be approximately a circle. Figure 4.10 shows the satellites and end bodies during 60 orbits in the orbital frame and Figure 4.11 shows the formation on the s_1-s_3 plane of the stroboscopic frame. Tethers between the satellites and the end bodies are not shown to simplify the figure. Simulation results of this configuration show that the tethered formation is stable up to 60 orbits. After 60 orbits the satellites in the formation depart from their initial position.

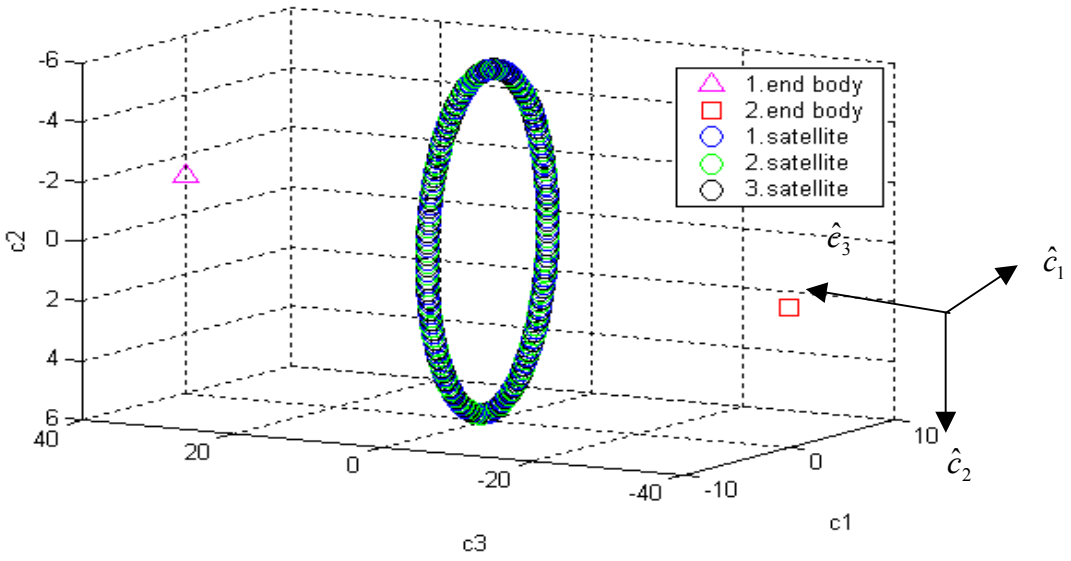

Figure 4.10 Formation During 60 Orbits in Orbital Frame

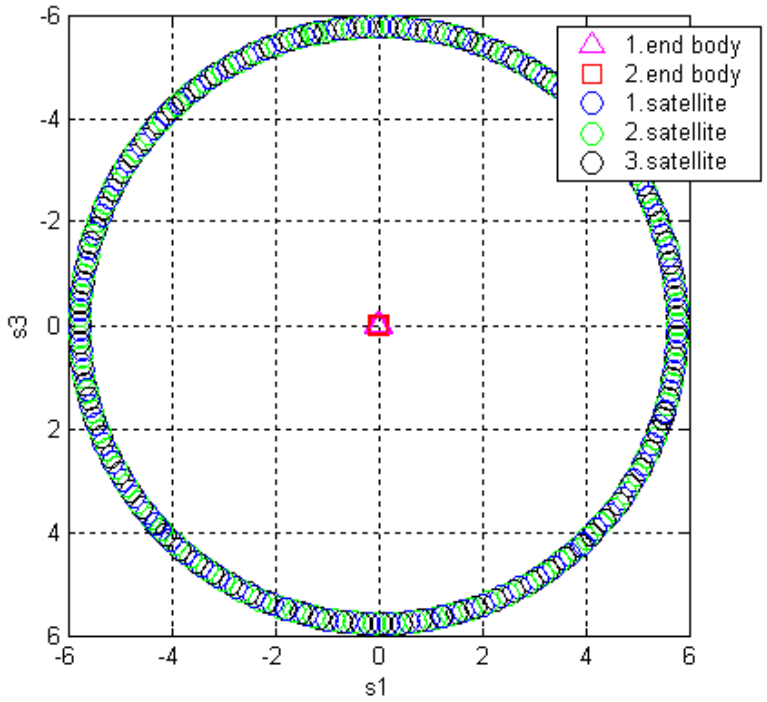

Figure 4.11 Positions of the Satellites and the End Bodies in the Stroboscopic Frame

4.4. Analysis of the Design Parameters

In this section the parameters that affect the stability of the tethered formation will be investigated. Stability of the tethered formation is affected by:

Spin rate of the formation

Mass ratio

Size of the formation

4.4.1. Spin Rate

Spin rate of the tethered formation changes the rotation angle, Φ, about the $\hat{c}_1$ axis. Increasing spin rate would decrease the rotation angle and the tethered formation will be less stable. Effects of the spin rate on the stability of the formation are investigated here for a different spin rate. The same mass and the size ratio of the reference configuration have been used.

For the spin rate $\nu_s = -3 * \omega_c$, half cone angle will be $\Phi = 87.2265$. This spin rate is higher than the spin rate, which is presented as a reference in the previous section. This configuration of the tethered formation is not stable for long period of time, and after the second orbit tethered formation begins to depart from the desired configuration. Figure 4.12 shows the positions of the satellites and the end bodies after the second orbit in orbital frame. Figure 4.13 shows the positions of the satellites and the end bodies in the stroboscopic frame for the same orbits.

This simulation demonstrates that the stability of the tethered formation decreases with the increasing spin rate with respect to the stroboscopic frame.

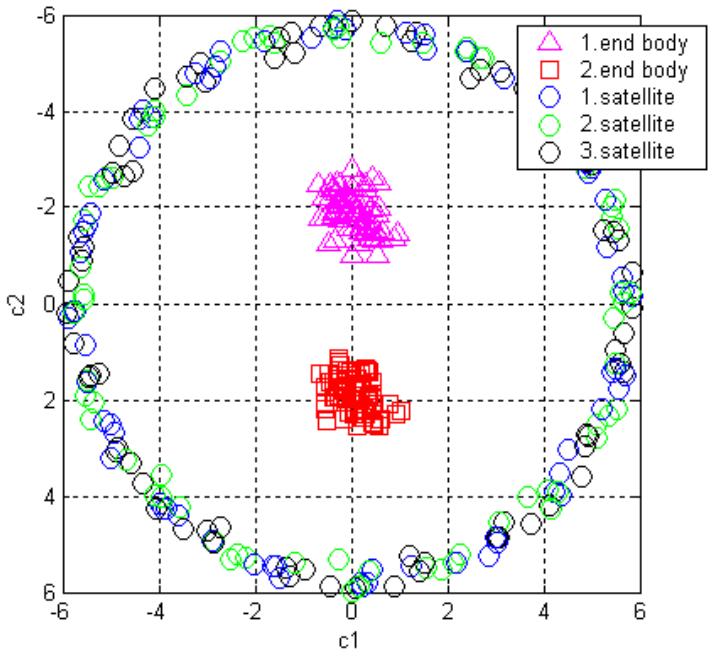

Figure 4.12 Positions of the Satellites and the End Bodies in The Orbital Frame for Higher Spin Rate

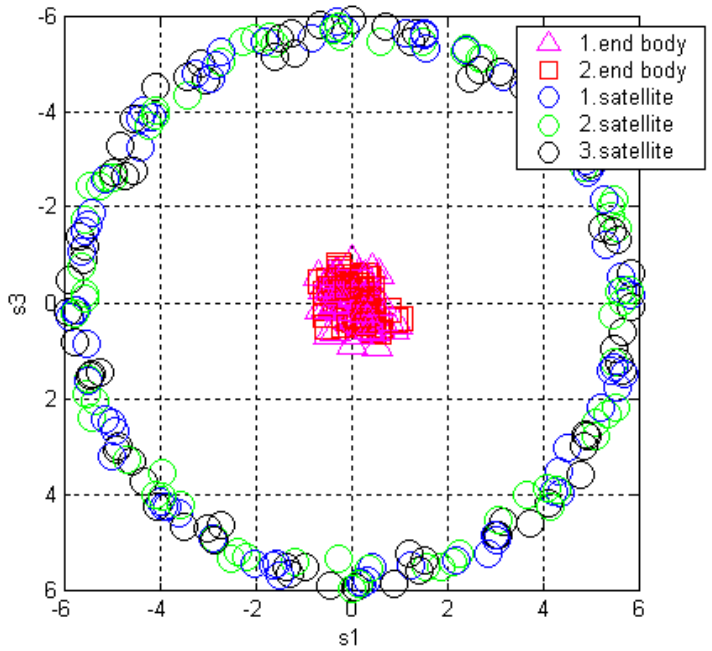

Figure 4.13 Positions of the Satellites and the End Bodies in The Stroboscopic Frame for Higher Spin Rate

For this configuration, satellites and the end bodies begin to depart from the initial position in the second orbit and for long period this deviation will be worse. This behavior of the tethered formation can be explained by the reduced half cone angle. The formation spin axis is farther from the nadir direction, so gravity gradient torques destabilize the system. Figure 4.14 shows the configuration of the tethered formation after 10 orbits.

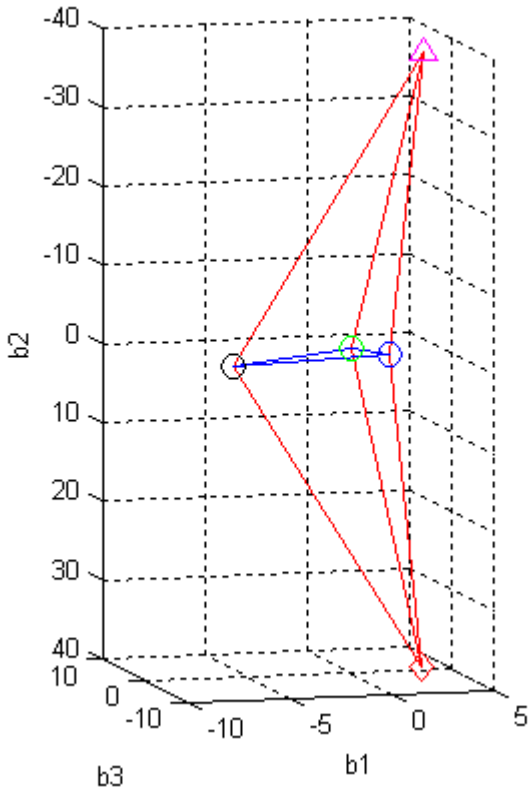

Figure 4.14 Tethered Formation with Higher Spin Rate
After 10 Orbits in Body Frame

4.4.2 Mass Ratio

The mass ratio of the tethered formation changes the minimum spin rate of the configurations and the inertia ratio, k_t. Different values for k_t cause a different half cone angle and orientation on the orbit. Effects of the mass ratio on the stability of the formation are investigated here for a different mass ratio. The same spin rate and the size ratio of the reference configuration have been used.

For the mass ratio $m_s / m_e = 3$, half cone angle will be $\Phi = 87.1810$. This mass ratio of m_s / m_e is higher than the mass ratio, which is presented as a reference in the previous section. The tethered configuration is not stable for long period of time. After the fifth orbit, the tethered formation begins to depart from the desired configuration. Figure 4.15 shows the positions of the satellites and the end bodies during eighth orbit in orbital frame. Figure 4.16 shows the positions of the satellites and the end bodies in stroboscopic frame.

This simulation demonstrates that the stability of the tethered formation decreases with the increasing mass ratio between the satellites and the end bodies.

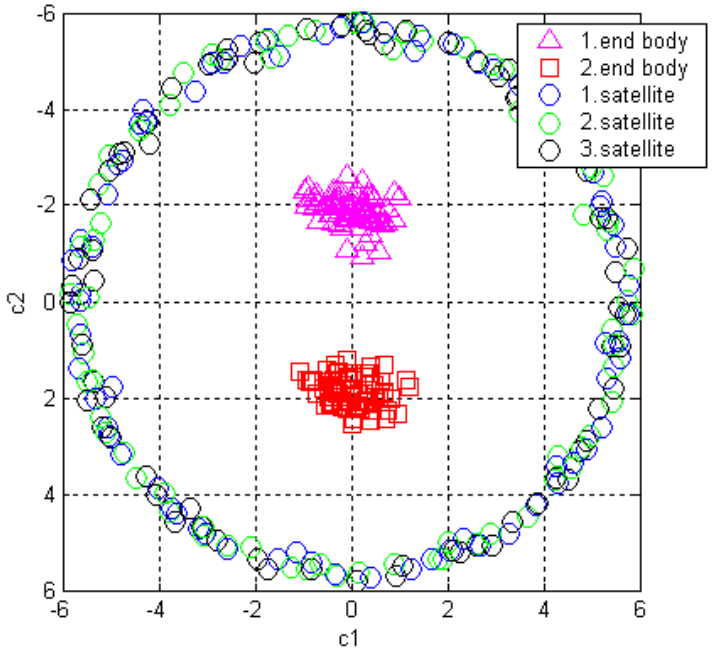

Figure 4.15 Positions of the Satellites and the End Bodies in the Orbital Frame for Higher Mass Ratio

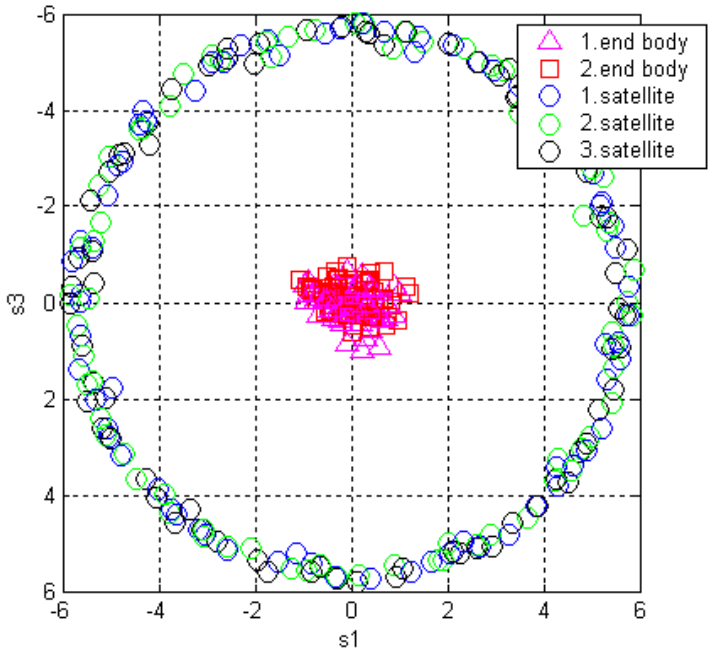

Figure 4.16 Positions of the Satellites and the End Bodies in The Stroboscopic Frame for Higher Mass Ratio

Figure 4.17 shows the tethered satellite formation configuration after 10 orbits.

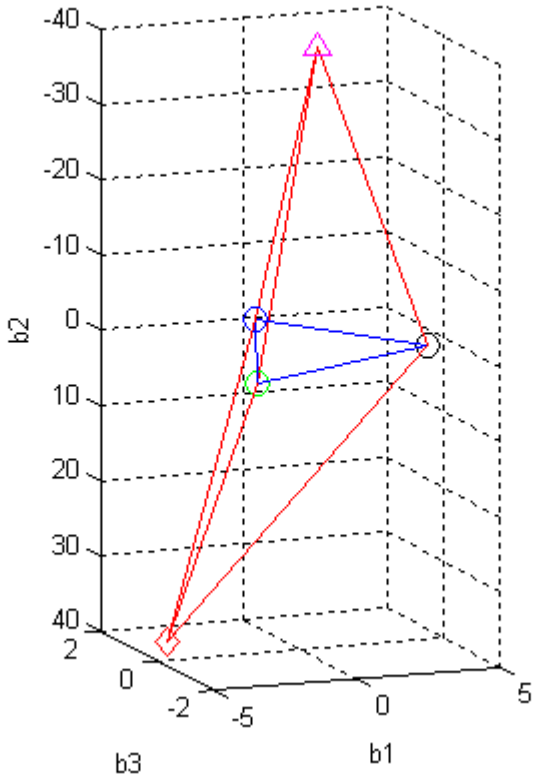

Figure 4.17 Tethered Formation with Higher Mass Ratio
After 20 Orbits in Body Frame

4.4.3. Size of the Formation

The size ratio of the tethered formation changes the value of the inertia ratio, k_t. Different values for k_t will cause a different half cone angle and orientation in the orbit. Effects of the size ratio on the stability of the formation are investigated here for a different size ratio. The same spin rate and the mass ratio of the reference configuration have been used.

For the size ratio L/D=9, half cone angle will be $\Phi = 88.5493$. This size ratio of L/D is higher than the size ratio, which is presented as a reference in the previous section. Figure 4.18 shows the positions of the satellites and the end bodies for three orbits between the 65 and the 68 orbits in the orbital frame. Figure 4.19 shows the positions of the satellites and the end bodies in the stroboscopic frame for the same orbits. After 68 orbits the shape of the formation begins to deform. This simulation demonstrates that the half cone angle increases with increasing size ratio and the angle between the spin axis and the nadir direction decreases with higher size ratio. Therefore increasing the size ratio increases the stability of the tethered formation.

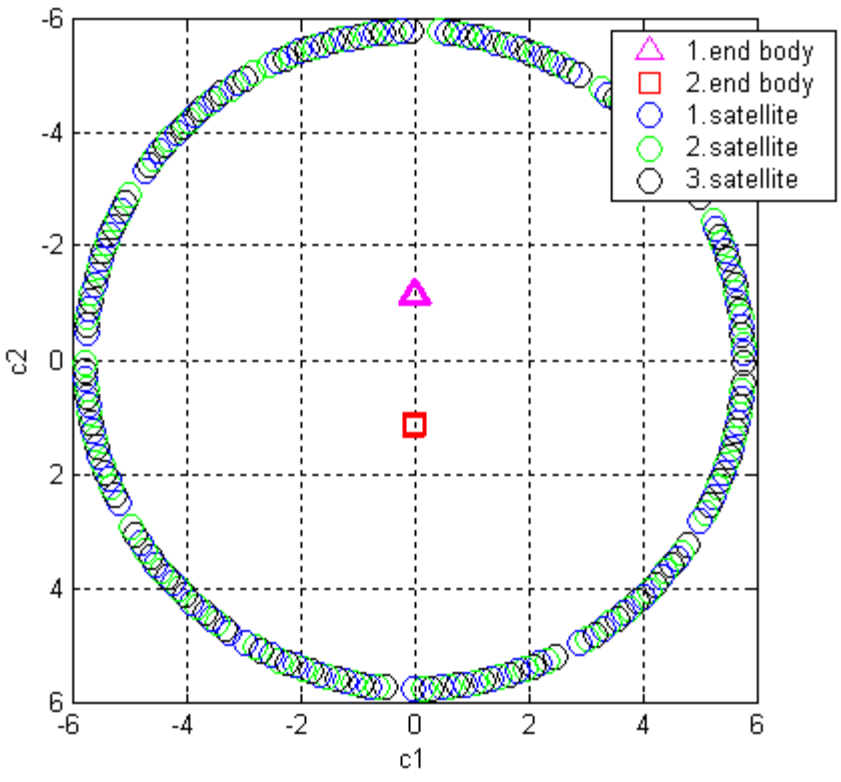

Figure 4.18 Positions of the Satellites and the End Bodies in the Orbital Frame for Higher Size Ratio

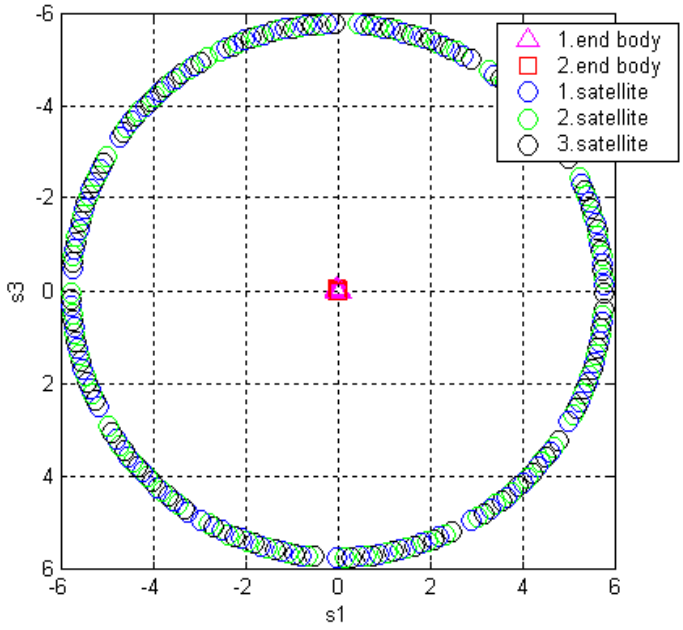

Figure 4.19 Positions of the Satellites and the End Bodies in the Stroboscopic Frame for Higher Size Ratio

Figure 4.20 shows the tethered satellite formation configuration after 80 orbits.

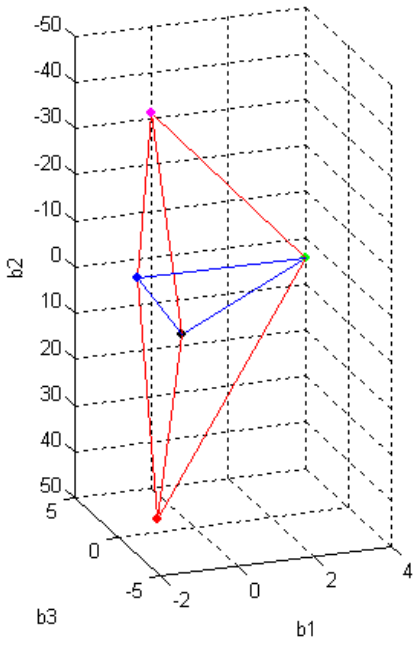

Figure 4.20 Tethered Formation with Higher Size Ratio After 80 Orbits in Body Frame

4.5 Stable Configurations

Simulation results show that the stability period of the tethered satellite formation depends on the configuration of the system. The half cone angle, which is the result of the design parameters, determines the stability of the tethered formation. Because of the gravity gradient force, configurations, which have the spin axis closer to the nadir direction, are more stable than the other configurations. The tethered formation which has the spin axis aligned with the nadir direction would be stable for very long time. However, to maintain such configuration is not possible for the non-rigid tethered satellite formation because of the minimum spin rate constraint.

Analysis shows that the stability decreases dramatically for the tethered formation configurations which have a half cone angle smaller than 88 degrees. Because of this a simulation has been set up to find the stable configurations with a minimum 88 degrees half cone angle; that is, the maximum deviation of the spin axis from the nadir direction is allowed to be 2 degrees. Figure 4.21 shows the stable configurations of tethered satellite formation with the half cone angle between $88^o$and 90^o degrees for the spin rate with respect to the stroboscopic frame on the order of the orbital rate, which is:

$$\hat{\nu}_s = \frac{\nu + \omega_c}{\omega_c} \tag{4.42}$$

and the size ratio of L/D in the range between 6 and 15. This plot supports the conclusions of the previous sections. The stability increases with larger L/D and lower spin rates (up to the minimum spin rate).

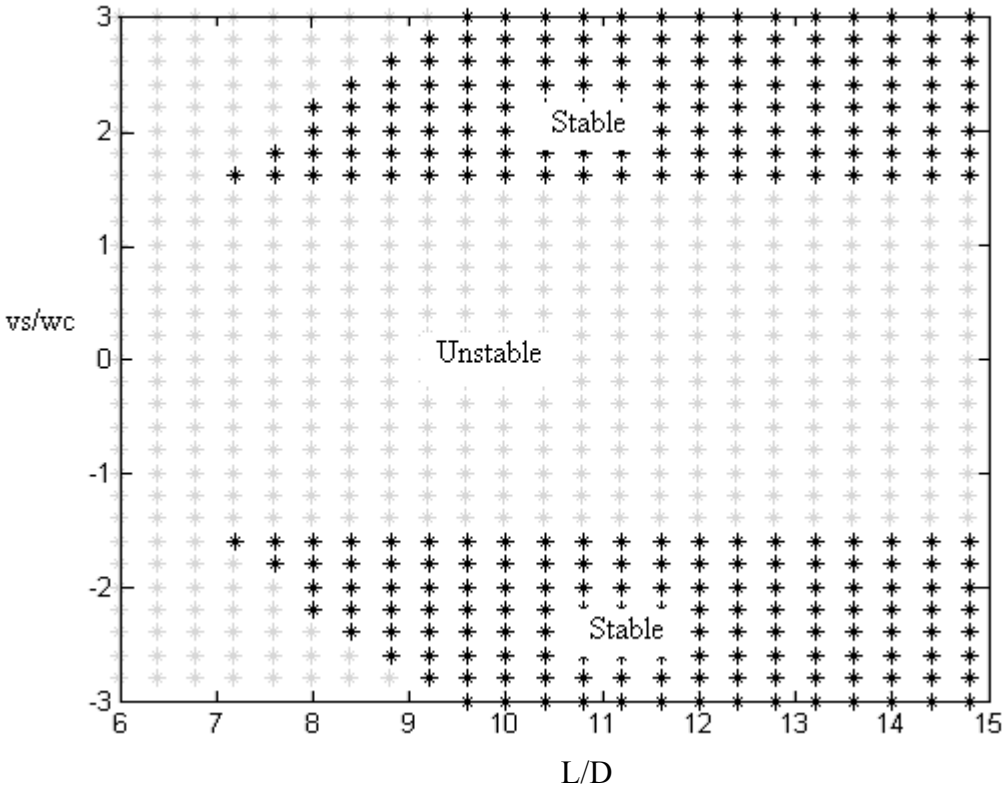

Figure 4.21 Stable Configurations

V. Conclusions and Recommendations

Likins-Pringle relative equilibrium has been analyzed for the possibility of using this equilibrium to find the stable configurations of the tethered formation about near-nadir directions. Since the application of the tethered formation is Earth surveillance and sensing, the system was designed so the sub satellites are widely distributed about the nadir directions. Two end bodies, which are placed at the opposite side of the triangular plane help for the system stability by using the gravity gradient force.

Stability of the tethered satellite system depends on several design parameters. Obtaining a stable tethered satellite formation with a spin axis perfectly aligned with the nadir direction is not possible. However it is possible to obtain a stable formation system, which has an angle between the spin axis and the nadir direction from very small values to about 2 degrees.

For this study the tethers between the satellites and the end bodies are considered as massless, extensible tethers. For the future study, the tethers should be modeled with one of the discritization methods to more accurately model the flexible nature of the tethers.

For this study the effects of the air drag, moon's gravitational force or the gravitational force of the sun are not considered. For the future study about the tethered satellite formation these perturbation forces should be taken into account and the effects of these forces on the stability of the tethered formation should be demonstrated.

Appendix A

Linearized Solution of the Equations of Motion

Equations of motion in the linearized form:

$$\begin{aligned}
&(\text{i}) \quad \ddot{\alpha}_1 + (1-k_t)\nu\dot{\alpha}_3 + k_t\nu^2\alpha_1 + 3\omega_c^2 k_t(\alpha_1 c + \alpha_3 s)c = 0 \\
&(\text{ii}) \quad \ddot{\alpha}_2 = 0 \\
&(\text{iii}) \quad \ddot{\alpha}_3 - (1-k_t)\nu\dot{\alpha}_1 + k_t\nu^2\alpha_3 + 3\omega_c^2 k_t(\alpha_1 c + \alpha_3 s)s = 0
\end{aligned} \tag{A.1}$$

where,

$$s = \sin(\nu + \omega_c)t \qquad c = \cos(\nu + \omega_c)t \qquad \omega_c = \sqrt{\frac{\mu}{R^3}} \quad \text{and}$$

$$k_t = \frac{I_a - I_t}{I_t} \tag{A.2}$$

The linearized equations of motion include time variable coefficient because of the nominal motion of the satellite and the reference spin rate. It is possible to simplify these equations by transforming them to a new set of coordinates that will eliminate the periodic coefficients. The new parameters are defined as [17]:

$$\begin{aligned}
&(\text{i}) \quad \gamma_1(t) \triangleq \alpha_1(t)\cos(\nu + \omega_c)t + \alpha_3(t)\sin(\nu + \omega_c)t \\
&(\text{ii}) \quad \gamma_2(t) \triangleq \alpha_2(t) \\
&(\text{iii}) \quad \gamma_3(t) \triangleq -\alpha_1(t)\sin(\nu + \omega_c)t + \alpha_3(t)\cos(\nu + \omega_c)t
\end{aligned} \tag{A.3}$$

Equation (A.1 i) implies that the satellite is unstable about the spin axis. Thus for the stability about the other two axis the equations of motion can be written in matrix form as:

$$\begin{bmatrix} 1 & 0 \\ 0 & 1 \end{bmatrix}\begin{bmatrix} \ddot{\alpha}_1 \\ \ddot{\alpha}_3 \end{bmatrix}+\begin{bmatrix} 0 & (1-k_t)\nu \\ -(1-k_t)\nu & 0 \end{bmatrix}\begin{bmatrix} \dot{\alpha}_1 \\ \dot{\alpha}_3 \end{bmatrix}+$$

$$\begin{bmatrix} 3\omega_c^2 k_t c^2 + k_t \nu^2 & 3\omega_c^2 k_t sc \\ 3\omega_c^2 k_t sc & 3\omega_c^2 k_t s^2 + k_t \nu^2 \end{bmatrix}\begin{bmatrix} \alpha_1 \\ \alpha_3 \end{bmatrix}=\begin{bmatrix} 0 \\ 0 \end{bmatrix} \tag{A.4}$$

And the new set of coordinates:

$$\begin{bmatrix} \gamma_1 \\ \gamma_2 \end{bmatrix}=\begin{bmatrix} c & s \\ -s & c \end{bmatrix}\begin{bmatrix} \alpha_1 \\ \alpha_3 \end{bmatrix} \tag{A.5}$$

Inverting and taking derivatives of this equation gives $\alpha_1, \alpha_3, \dot{\alpha}_1, \dot{\alpha}_3, \ddot{\alpha}_1, \ddot{\alpha}_3$ in terms of the new set of coordinates $\gamma_1, \gamma_3, \dot{\gamma}_1, \dot{\gamma}_3, \ddot{\gamma}_1, \ddot{\gamma}_3$:

$$\begin{bmatrix} \alpha_1 \\ \alpha_2 \end{bmatrix}=\begin{bmatrix} c & -s \\ s & c \end{bmatrix}\begin{bmatrix} \gamma_1 \\ \gamma_3 \end{bmatrix} \tag{A.6}$$

By taking the derivative of the equation (A.6):

$$\begin{bmatrix} \dot{\alpha}_1 \\ \dot{\alpha}_3 \end{bmatrix}=\begin{bmatrix} c & -s \\ s & c \end{bmatrix}\begin{bmatrix} \dot{\gamma}_1 \\ \dot{\gamma}_3 \end{bmatrix}+p\begin{bmatrix} -s & -c \\ c & -s \end{bmatrix}\begin{bmatrix} \gamma_1 \\ \gamma_3 \end{bmatrix} \tag{A.7}$$

where,

$$p=(\nu+\omega_c) \tag{A.8}$$

And the second derivative of this equation is:

$$\begin{bmatrix} \ddot{\alpha}_1 \\ \ddot{\alpha}_3 \end{bmatrix}=\begin{bmatrix} c & -s \\ s & c \end{bmatrix}\begin{bmatrix} \ddot{\gamma}_1 \\ \ddot{\gamma}_3 \end{bmatrix}+p\begin{bmatrix} -s & -c \\ c & -s \end{bmatrix}\begin{bmatrix} \dot{\gamma}_1 \\ \dot{\gamma}_3 \end{bmatrix}+p\begin{bmatrix} -s & -c \\ c & -s \end{bmatrix}\begin{bmatrix} \dot{\gamma}_1 \\ \dot{\gamma}_3 \end{bmatrix}+p^2\begin{bmatrix} -c & s \\ -s & -c \end{bmatrix}\begin{bmatrix} \gamma_1 \\ \gamma_3 \end{bmatrix}$$

By adding the similar terms:

$$\begin{bmatrix} \ddot{\alpha}_1 \\ \ddot{\alpha}_3 \end{bmatrix} = \begin{bmatrix} c & -s \\ s & c \end{bmatrix} \begin{bmatrix} \ddot{\gamma}_1 \\ \ddot{\gamma}_3 \end{bmatrix} + 2p \begin{bmatrix} -s & -c \\ c & -s \end{bmatrix} \begin{bmatrix} \dot{\gamma}_1 \\ \dot{\gamma}_3 \end{bmatrix} + p^2 \begin{bmatrix} -c & s \\ -s & -c \end{bmatrix} \begin{bmatrix} \gamma_1 \\ \gamma_3 \end{bmatrix} \tag{A.9}$$

Substituting the equations for, $\begin{bmatrix} \alpha_1 \\ \alpha_3 \end{bmatrix}, \begin{bmatrix} \dot{\alpha}_1 \\ \dot{\alpha}_3 \end{bmatrix}, \begin{bmatrix} \ddot{\alpha}_1 \\ \ddot{\alpha}_3 \end{bmatrix}$ into the equations of motion yields:

$$\begin{bmatrix} c & -s \\ s & c \end{bmatrix} \begin{bmatrix} \ddot{\gamma}_1 \\ \ddot{\gamma}_3 \end{bmatrix} + 2p \begin{bmatrix} -s & -c \\ c & -s \end{bmatrix} \begin{bmatrix} \dot{\gamma}_1 \\ \dot{\gamma}_3 \end{bmatrix} + p^2 \begin{bmatrix} -c & s \\ -s & -c \end{bmatrix} \begin{bmatrix} \gamma_1 \\ \gamma_3 \end{bmatrix} +$$

$$\begin{bmatrix} 0 & (1-k_t)\nu \\ -(1-k_t)\nu & 0 \end{bmatrix} \begin{bmatrix} c & -s \\ s & c \end{bmatrix} \begin{bmatrix} \dot{\gamma}_1 \\ \dot{\gamma}_3 \end{bmatrix} + p \begin{bmatrix} -s & -c \\ c & -s \end{bmatrix} \begin{bmatrix} 0 & (1-k_t)\nu \\ -(1-k_t)\nu & 0 \end{bmatrix} \begin{bmatrix} \gamma_1 \\ \gamma_3 \end{bmatrix} +$$

$$\begin{bmatrix} 3\omega_c^2 k_t c^2 + k_t \nu^2 & 3\omega_c^2 k_t sc \\ 3\omega_c^2 k_t sc & 3\omega_c^2 k_t s^2 + k_t \nu^2 \end{bmatrix} \begin{bmatrix} c & -s \\ s & c \end{bmatrix} \begin{bmatrix} \gamma_1 \\ \gamma_3 \end{bmatrix} = \begin{bmatrix} 0 \\ 0 \end{bmatrix} \tag{A.10}$$

Note that:

$$\begin{bmatrix} c & s \\ -s & c \end{bmatrix} \begin{bmatrix} -s & -c \\ c & -s \end{bmatrix} = \begin{bmatrix} 0 & -c^2 - s^2 \\ c^2 + s^2 & 0 \end{bmatrix} = \begin{bmatrix} 0 & -1 \\ 1 & 0 \end{bmatrix} \tag{A.11}$$

Thus:

$$\begin{bmatrix} -s & -c \\ c & -s \end{bmatrix} = \begin{bmatrix} c & -s \\ s & c \end{bmatrix} \begin{bmatrix} 0 & -1 \\ 1 & 0 \end{bmatrix} \tag{A.12}$$

Substituting the equation (A.12) into the equation (A.10):

$$\begin{bmatrix} c & -s \\ s & c \end{bmatrix} \left\{ \begin{bmatrix} \ddot{\gamma}_1 \\ \ddot{\gamma}_3 \end{bmatrix} + 2p \begin{bmatrix} 0 & -1 \\ 1 & 0 \end{bmatrix} \begin{bmatrix} \dot{\gamma}_1 \\ \dot{\gamma}_3 \end{bmatrix} - p^2 \begin{bmatrix} \gamma_1 \\ \gamma_3 \end{bmatrix} + \begin{bmatrix} 0 & (1-k_t)\nu \\ -(1-k_t)\nu & 0 \end{bmatrix} \begin{bmatrix} \dot{\gamma}_1 \\ \dot{\gamma}_3 \end{bmatrix} + \right.$$

$$\left. p \begin{bmatrix} 0 & -1 \\ 1 & 0 \end{bmatrix} \begin{bmatrix} 0 & (1-k_t)\nu \\ -(1-k_t)\nu & 0 \end{bmatrix} \begin{bmatrix} \gamma_1 \\ \gamma_3 \end{bmatrix} + \begin{bmatrix} 3\omega_c^2 k_t + k_t \nu^2 & 0 \\ 0 & k_t \nu^2 \end{bmatrix} \begin{bmatrix} \gamma_1 \\ \gamma_3 \end{bmatrix} \right\} = \begin{bmatrix} 0 \\ 0 \end{bmatrix} \tag{A.13}$$

Simplifying the equation (A.13):

$$\begin{bmatrix} c & -s \\ s & c \end{bmatrix}\left\{\begin{bmatrix} \ddot{\gamma}_1 \\ \ddot{\gamma}_3 \end{bmatrix}+\begin{bmatrix} 0 & -2p+(1-k_t)\nu \\ 2p-(1-k_t) & 0 \end{bmatrix}\begin{bmatrix} \dot{\gamma}_1 \\ \dot{\gamma}_3 \end{bmatrix}+\right.$$

$$\left.\begin{bmatrix} -p^2+p(1-k_t)\nu+3\omega_c^2 k_t+k_t\nu & 0 \\ 0 & -p^2+p(1-k_t)\nu+k_t\nu^2 \end{bmatrix}\begin{bmatrix} \gamma_1 \\ \gamma_3 \end{bmatrix}\right\}=\begin{bmatrix} 0 \\ 0 \end{bmatrix} \quad \text{(A.14)}$$

Since:

$$\det\begin{bmatrix} c & -s \\ s & c \end{bmatrix}=1\neq 0 \quad \text{(A.15)}$$

The term in the parenthesis in the equation (A.14) must be equal to zero to satisfy the equation:

$$\left\{\begin{bmatrix} \ddot{\gamma}_1 \\ \ddot{\gamma}_3 \end{bmatrix}+\begin{bmatrix} 0 & -2p+(1-k_t)\nu \\ 2p-(1-k_t) & 0 \end{bmatrix}\begin{bmatrix} \dot{\gamma}_1 \\ \dot{\gamma}_3 \end{bmatrix}+\right.$$

$$\left.\begin{bmatrix} -p^2+p(1-k_t)\nu+3\omega_c^2 k_t+k_t\nu & 0 \\ 0 & -p^2+p(1-k_t)\nu+k_t\nu^2 \end{bmatrix}\begin{bmatrix} \gamma_1 \\ \gamma_3 \end{bmatrix}\right\}=\begin{bmatrix} 0 \\ 0 \end{bmatrix} \quad \text{(A.15)}$$

Substituting the equation (A.8) into the equation (A.15):

$$p=(\nu+\omega_c)$$

Elements of the equation become:

$$\begin{aligned} -2p+(1-k_t)\nu &= -2(\nu+\omega_c)+(1-k_t)\nu \\ &= -(\nu+2\omega_c+k_t\nu) \end{aligned} \quad \text{(A.16)}$$

$$\begin{aligned} 2p-(1-k_t)\nu &= 2(\nu+\omega_c)-(1-k_t)\nu \\ &= \nu+2\omega_c+k_t\nu \end{aligned} \quad \text{(A.17)}$$

$$\begin{aligned} -p^2+p(1-k_t)\nu+3\omega_c^2 k_t+k_t\nu &= -(\nu+\omega_c)^2+(\nu+\omega_c)(1-k_t)\nu+3\omega_c^2 k_t+k_t\nu \\ &= -\nu\omega_c-\omega_c^2-k_t\nu\omega_c+3k_t\omega_c^2 \\ &= k_t(3\omega_c^2-\nu\omega_c)-\omega_c(\nu+\omega_c) \end{aligned} \quad \text{A.18)}$$

$$
\begin{aligned}
-p^2 + p(1-k_t)\nu + k_t\nu^2 &= -(\nu+\omega_c)^2 + (\nu+\omega_c)(1-k_t)\nu + k_t\nu^2 \\
&= -\nu\omega_c - \omega_c^2 - k_t\nu\omega_c \\
&= -(k_t\nu\omega_c + \omega_c(\nu+\omega_c))
\end{aligned}
\tag{A.19}
$$

Substitute the equations (A.16) through (A.19) into the equation (A.15), equation of motion in the matrix form becomes:

$$
\begin{bmatrix} \ddot{\gamma}_1 \\ \ddot{\gamma}_3 \end{bmatrix} + \begin{bmatrix} 0 & -(\nu + 2\omega_c + k_t\nu) \\ (\nu + 2\omega_c + k_t\nu) & 0 \end{bmatrix} \begin{bmatrix} \dot{\gamma}_1 \\ \dot{\gamma}_3 \end{bmatrix} + \begin{bmatrix} k_t(3\omega_c^2 - \nu\omega_c) - \omega_c(\nu+\omega_c) & 0 \\ 0 & -(k_t\nu\omega_c + \omega_c(\nu+\omega_c)) \end{bmatrix} \begin{bmatrix} \gamma_1 \\ \gamma_3 \end{bmatrix} = \begin{bmatrix} 0 \\ 0 \end{bmatrix}
\tag{A.20}
$$

Finally the equations of motion can be written as:

$$
\begin{aligned}
&(\text{i}) \quad \ddot{\gamma}_1 - (\nu + 2\omega_c + k_t\nu)\dot{\gamma}_3 + (k_t(3\omega_c^2 - \nu\omega_c) - \omega_c(\nu+\omega_c))\gamma_1 = 0 \\
&(\text{ii}) \quad \ddot{\gamma}_2 = 0 \\
&(\text{iii}) \quad \ddot{\gamma}_3 + (\nu + 2\omega_c + k_t\nu)\dot{\gamma}_1 - -(k_t\nu\omega_c + \omega_c(\nu+\omega_c))\gamma_3 = 0
\end{aligned}
\tag{A.21}
$$

Appendix B

Rotation Matrix

All vectors represented by their components with respect to the reference frame. This representation is relative to the selected reference frame, and it is possible to write the same vector with respect to another reference frame. To write the vector in another reference frame, transformation is used between these reference frames. Rotation matrix gives the transformation of any reference frame to another. Elements of the rotation matrix show the relationship between the axes of two reference frames, and they are the cosine of the angles between each axes of the reference frames. Because of this, rotation matrix is also called as the direction cosine matrix [18].

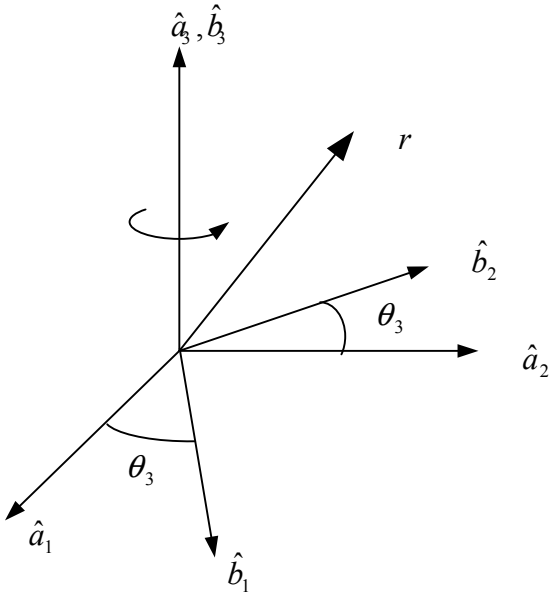

Figure B.1 Rotation of the Reference Frame

$$\bar{r}^{\,a} = r_{a1}\hat{a}_1 + r_{a2}\hat{a}_2 + r_{a3}\hat{a}_3 \tag{B.1}$$

The term $\bar{r}^{\,a}$ is the representation of $\bar{r}$ vector in F_a frame.

$$\bar{r}^{\,b} = r_{b1}\hat{b}_1 + r_{b2}\hat{b}_2 + r_{b3}\hat{b}_3 \tag{B.2}$$

The term $\bar{r}^{\,b}$ is the representation of $\bar{r}$ vector in F_b frame. Transformation between the F_a frame and F_b frame can be shown by using the rotation matrix:

$$F_b = R^{ba}F_a \quad \text{where } R^{ba} \text{ is the rotation matrix } \quad R^{ba} = \begin{bmatrix} c_{11} & c_{12} & c_{13} \\ c_{21} & c_{22} & c_{23} \\ c_{31} & c_{32} & c_{33} \end{bmatrix} \tag{B.3}$$

$$\begin{bmatrix} \hat{b}_1 \\ \hat{b}_2 \\ \hat{b}_3 \end{bmatrix} = \begin{bmatrix} c_{11} & c_{12} & c_{13} \\ c_{21} & c_{22} & c_{23} \\ c_{31} & c_{32} & c_{33} \end{bmatrix} \begin{bmatrix} \hat{a}_1 \\ \hat{a}_2 \\ \hat{a}_3 \end{bmatrix} \tag{B.4}$$

From the equation above, the relation between these two frames F_a and F_b can be written for each $\hat{b}_1$, $\hat{b}_2$ and $\hat{b}_3$ [17]:

$$\text{(i)} \quad \hat{b}_1 = c_{11}\hat{a}_1 + \hat{c}_{12}\hat{a}_2 + c_{13}\hat{a}_3$$

$$\text{(ii)} \quad \hat{b}_2 = c_{21}\hat{a}_1 + \hat{c}_{22}\hat{a}_2 + c_{23}\hat{a}_3$$

$$\text{(iii)} \quad \hat{b}_3 = c_{31}\hat{a}_1 + \hat{c}_{32}\hat{a}_2 + c_{33}\hat{a}_3 \tag{B.5}$$

By using the cross product rule equations for the relation between the axis can be written:

$$\hat{a}_1 \; x \; \hat{a}_2 = \hat{a}_3 \qquad \hat{a}_2 \; x \; \hat{a}_3 = \hat{a}_1 \qquad \hat{a}_3 \; x \; \hat{a}_1 = \hat{a}_2 \tag{B.6}$$

$$\hat{b}_1 \; x \; \hat{b}_2 = \hat{b}_3 \qquad \hat{b}_2 \; x \; \hat{b}_3 = \hat{b}_1 \qquad \hat{b}_3 \; x \; \hat{b}_1 = \hat{b}_2 \tag{B.7}$$

From the equations (B.5):

$$\hat{b}_1 = \hat{b}_2 \; x \; \hat{b}_3$$

$$\hat{b}_1 = (c_{21}\hat{a}_1 + c_{22}\hat{a}_2 + c_{23}\hat{a}_3) \; x \; (c_{31}\hat{a}_1 + c_{32}\hat{a}_2 + c_{33}\hat{a}_3)$$

$$\hat{b}_1 = (c_{22}c_{33} - c_{23}c_{32})\hat{a}_1 + (c_{23}c_{31} - c_{21}c_{33})\hat{a}_2 + (c_{21}c_{32} - c_{22}c_{31})\hat{a}_3 \qquad \text{(B.8)}$$

$$\hat{b}_2 = \hat{b}_3 \; x \; \hat{b}_1$$

$$\hat{b}_2 = (c_{31}\hat{a}_1 + c_{32}\hat{a}_2 + c_{33}\hat{a}_3) \; x \; (c_{11}\hat{a}_1 + c_{12}\hat{a}_2 + c_{13}\hat{a}_3)$$

$$\hat{b}_2 = (c_{32}c_{13} - c_{33}c_{12})\hat{a}_1 + (c_{33}c_{11} - c_{31}c_{13})\hat{a}_2 + (c_{31}c_{12} - c_{32}c_{11})\hat{a}_3 \qquad \text{(B.9)}$$

$$\hat{b}_3 = \hat{b}_1 \; x \; \hat{b}_2$$

$$\hat{b}_3 = (c_{11}\hat{a}_1 + c_{12}\hat{a}_2 + c_{13}\hat{a}_3) \; x \; (c_{21}\hat{a}_1 + c_{22}\hat{a}_2 + c_{23}\hat{a}_3)$$

$$\hat{b}_3 = (c_{12}c_{23} - c_{13}c_{22})\hat{a}_1 + (c_{13}c_{21} - c_{11}c_{23})\hat{a}_2 + (c_{11}c_{22} - c_{12}c_{21})\hat{a}_3 \qquad \text{(B.10)}$$

With the equations above, nine relationships between the elements of rotation matrix can be defined [17]:

$$c_{11} = c_{22}c_{33} - c_{23}c_{32} \qquad c_{21} = c_{32}c_{13} - c_{33}c_{12}$$

$$c_{12} = c_{23}c_{31} - c_{21}c_{33} \qquad c_{22} = c_{33}c_{11} - c_{31}c_{13}$$

$$c_{13} = c_{21}c_{32} - c_{22}c_{31} \qquad \text{(B.11)} \qquad c_{23} = c_{31}c_{12} - c_{32}c_{11} \qquad \text{(B.12)}$$

$$c_{31} = c_{12}c_{23} - c_{13}c_{22}$$

$$c_{32} = c_{13}c_{21} - c_{11}c_{23}$$

$$c_{33} = c_{11}c_{22} - c_{12}c_{21} \qquad \text{(B.13)}$$

Bibliography

1. Luu, Kim and others "University Nanosatellite Distributed Satellite Capabilities to Support Techsat 21." *AIAA/USU Small Satellite Conference*, Logan,Utah, August 1999.

2. Irvin, David J. *A study of Linear vs. Nonlinear Control Techniques for the Reconfiguration of Satellite Formations*. MS thesis, AFIT/GA/ENY/01M-02, graduate School of Engineering, Air Force Institute of Technology (AU), Wright-Patterson AFB OH, march 2001.

3. "Birds Inspire Formation-Flying Satellites." *U.S. Air Force News Release*, 4 July 2000.

4. Tragesser, Steven G. "Formation Flying With Tethered Spacecraft." *AIAA/AAS Astrodynamics Specialist Conference.* AIAA 2000-4133. Denver, Colorado. August 2000.

5. Cicci, D. A., Lovell, T. A. and Qualls, C. "A Method for the Identification of a Tethered Satellite." *Advances in the Astronautical Sciences*. Vol.102, Part II, p.1399-1417. AAS 99-196. San Diego. California: Univelt, Incorporated.1999.

6. Cho, S., Cochran Jr., J. E. and Cicci, D. A. "Approximate Solutions for Tethered Satellite Motion." *Advances in the Astronautical Sciences*. Vol.102, Part II, p.1345-1359. AAS 99-193. San Diego. California: Univelt, Incorporated.1999.

7. Beletsky, Viladimir V. and Levin, Evgenii M. Dynamics of Space Tether Systems. *Advances in the Astronautical Sciences.* Vol.83. San Diego. California: Univelt, Incorporated.1993.

8. Biswell, Brian L. and Puig-Suari, Jordi. "Improved Tether Aerobraking Maneuvers Using a LiftingProbe." *Advances in the Astronautical Sciences*. Vol.103, Part II, p.1739-1760. AAS 99-412. San Diego. California: Univelt, Incorporated.2000.

9. Meirovitch, Leonard. *Elements of Vibration Analysis*. New York: McGraw-Hill Inc. 1986.

10. Meirovitch, Leonard. *Computational Methods in Structural Dynamics*. The Netherlands: Sijthoff and Nordhoff International Publishers B.V. 1980.

11. Biosbroek, Robin G. J. and Crellin, Ean B. "On the Validity of a Simple Bead-Model for Tethered Systems." *50th International Astronautical Congress*. IAF-99-A5.02. Amsterdam, The Netherlands. 4-8 Oct. 1999.

12. Modi, V. J., Lakshmanan, P. K. and Misra, A. K. "Dynamics and Control of Tethered Spacecraft During Deployment and Retrieval." *Mechanics and Control of Large Flexible Structures.* A91-54451 23-39. Washington. DC.

13. Takeichi, Noboru and others. "Dynamic Behavior of a Tethered System with Multi-Subsatellites in Elliptical Orbits." *AIAA/ASME/ASCE/AHS/ASC Structures, Structural Dynamics and Materials Conference and Exhibit*. AIAA 2000-1776. Atlanta, GA. 3-6 April 2000.

14. Zhu, Renzhang , Lei, Da , Lin, Huabao and Misra, A. K. "Attitude Dynamics of Tethered Systems." *49th International Astronautical Congress*. IAF-98-A5.03. Melbourne, Australia. 28 Sept -2 Oct. 1998.

15. Kalantzis, S. , Modi, V. J. , Pradhan, S. and Misra, A. K. "Order-N Formulation and Dynamics of Multibody Tethered Systems." *Journal of Guidance, Control and Dynamics.* Vol.21, No.2, p.277-285. April 1998.

16. DeCou, Anthony B. "Tether Static Shape for Rotating Multimass, Multitether, Spacecraft for 'Triangle' Michelson Interferometer." *Journal of Guidance, Control and Dynamics.* Vol.12, No.2, p.273-275. March 1989.

17. Hughes, Peter C. *Spacecraft Attitude Dynamics*. New York: John Wiley and Sons.1986.

18. Wiesel, William E. *Spaceflight Dynamics (2nd edition)*. Boston, MA: Irwin McGraw-Hill. 1997.

19. Chobotov, Viladimir A. *Orbital Mechanics (2nd edition)*. Virginia: American Institute of Aeronautics and Astronautics. Inc. 1996.

20. Williams, Trevor and Moore, Kenneth. "Dynamics of Tethered Satellite Formations". *AAS/AIAA space Flight Mechanics Meeting*. AAS 02-198. San Antonio, Texas. 27-30 January 2002.

REPORT DOCUMENTATION PAGE

Form Approved
OMB No. 074-0188

1. REPORT DATE *(DD-MM-YYYY)*	2. REPORT TYPE	3. DATES COVERED *(From – To)*
26-03-2002	**Master's Thesis**	Sep 2000 – Mar 2002

4. TITLE AND SUBTITLE

STABILITY OF A TETHERED SATELLITE FORMATION ABOUT THE LIKINS-PRINGLE EQUILIBRIA

5a. CONTRACT NUMBER

5b. GRANT NUMBER

5c. PROGRAM ELEMENT NUMBER

6. AUTHOR(S)

Tuncay, Ayhan, 1LT, TUAF

5d. PROJECT NUMBER

5e. TASK NUMBER

5f. WORK UNIT NUMBER

7. PERFORMING ORGANIZATION NAMES(S) AND ADDRESS(S)

Air Force Institute of Technology
Graduate School of Engineering and Management (AFIT/ENY)
2950 P Street, Building 640
WPAFB OH 45433-7765

8. PERFORMING ORGANIZATION REPORT NUMBER

AFIT/GSO/ENY/02-4

9. SPONSORING/MONITORING AGENCY NAME(S) AND ADDRESS(ES)

Kenneth T Moore, Ph.D.
Sheet Dynamics, Ltd.
Suite 170
1776 Mentor Avenue
Cincinnati, OH 45212

10. SPONSOR/MONITOR'S ACRONYM(S)

11. SPONSOR/MONITOR'S REPORT NUMBER(S)

12. DISTRIBUTION/AVAILABILITY STATEMENT

APPROVED FOR PUBLIC RELEASE; DISTRIBUTION UNLIMITED.

13. SUPPLEMENTARY NOTES

14. ABSTRACT

Previous efforts have been directed at the guidance and control of free flying satellites clusters using reaction thrusters. A Tethered Formation of Satellites has great potential to enhance surveillance and imaging of earth objects. To maintain the shape of formation and keep the tethers in tension, the system needs to be spinning. General study has been focused on a planar formation and the results showed that Earth pointing configurations are not stable. This study demonstrates that spin stabilization and the use of gravity gradient for formation flight with tethered satellites reduce the necessity of thrusters for station keeping maneuvers. A tethered satellite formation, which consists of three satellites at the corners of an equilateral triangle, and two end bodies at the opposite side of this triangular plane is studied to obtain the stability based on the Likins-Pringle relative equilibrium for rigid satellites, for long period. Depending on the size of the formation and the mass ratio of the satellites to end bodies, tethered satellite formation showed that long-term stability is achievable for a continuously earth-pointing system.

15. SUBJECT TERMS

Tethered Formation, Formation Flight, Tethered Satellites, Likins-Pringle Equilibrium

16. SECURITY CLASSIFICATION OF:			17. LIMITATION OF ABSTRACT	18. NUMBER OF PAGES	19a. NAME OF RESPONSIBLE PERSON
a. REPORT	b. ABSTRACT	c. THIS PAGE			Steve G. Tragesser, Assistant Professor, AFIT/ENY
U	U	U	UU	88	19b. TELEPHONE NUMBER *(Include area code)* 785-6565 ext.4286 Steven.Tragesser@Afit.Edu

Standard Form 298 (Rev. 8-98)
Prescribed by ANSI Std. Z39-18